

had returned to basal level by 24 and 48 h after exposure, respectively. We next investigated the status of protein biosynthesis in resistant and parental cells. Newly synthesized proteins were labeled and measured before and after bortezomib treatment (Supplementary Materials and methods and Supplementary Figure S5). After bortezomib treatment, the two parental lines continued to synthesize protein 6 h after treatment but this was reduced by 24 h because of progressive apoptosis. In contrast, the two resistant lines both maintained continuous protein synthesis throughout the treatment. These results suggest that bortezomib-resistant MM cells maintain the same level of protein synthesis, unlike the bortezomib-adapted myeloid leukemia HL60a cell that was previously reported.¹⁸ We also determined the expression levels of each of the 20S proteasome subunits, $\beta 1$, $\beta 2$ and $\beta 5$. The total amount of all three subunits was comparable between resistant and parental cells before bortezomib exposure (Figure 2c). Only the amount of $\beta 2$ subunit was slightly increased after bortezomib treatment in the resistant cells, whereas it was gradually decreased in the parental cells.

We next investigated the dose-dependent alteration of accumulated polyubiquitinated proteins and expression levels of CHOP and Noxa, and activation of caspase-3, in bortezomib-resistant and parental MM cells treated with the drug. At a higher concentration of bortezomib than the IC_{50} value, the two resistant lines showed activation of caspase-3 and Noxa expression, indicating progression to apoptosis. However, they showed moderate accumulation of polyubiquitinated proteins, which was not followed by activation of CHOP. This finding may indicate that intracellular stresses different from proteasome inhibition have occurred, which trigger apoptosis independently of ER stress before excessive unfolded protein accumulation can take place at high concentrations of bortezomib.

To compare bortezomib-induced proteasome inhibition, chymotrypsin-like activity was measured. This was found to decrease in KMS-11 cells to 30–37% of the control level after a 6-h exposure, whereas KMS-11/BTZ cells retained 47–51% of the activity even after a 48-h exposure. In OPM-2 cells, chymotrypsin-like activity on 6-h exposure was reduced to 10–13%, whereas OPM-2/BTZ cells retained 21–23% of the level in unexposed cells and maintained that until 48 h after exposure. These results indicate that the degree of proteasome inhibition is slightly weaker in bortezomib-resistant cells than their parental cells after bortezomib exposure. This subtle difference may contribute to the avoidance of fatal unfolded protein accumulation.

Expression levels of ubiquitin specific proteases, a lysosomal protease,¹⁸ before and after bortezomib exposure were also examined. As shown in Supplementary Figure S5 (also refer Supplementary Materials and methods), neither bortezomib-resistant line overexpressed USPs before or after exposure to bortezomib compared with their parental cells. This indicates that USPs have little effect in compensating for impaired proteasome activity in bortezomib-resistant cells.

Alteration of the proteasome $\beta 5$ subunit in bortezomib-resistant MM cells

Most recently, mutation of the *PSMB5* gene (G322A) has been proposed as a possible mechanism responsible for bortezomib resistance in T-cell lymphoblastic/leukemia and myeloid leukemia cells adapted to bortezomib treatment.^{16,17} To investigate the presence or absence of genetic alterations in the *PSMB5* gene in our MM cells, exon 2 encoding the conserved bortezomib-binding pocket regions in the $\beta 5$ subunit was sequenced. As shown in Figures 2d and a, substitution at

nucleotide position 322 (G/A), which corresponds to the amino-acid change (Ala49Thr) same as previously reported,^{16,17} was identified in both the bortezomib-resistant MM cell lines, but not in the parental cells. This reflects the appearance of a G322A-mutated allele in addition to the remaining wild-type allele in bortezomib-resistant MM cells.

The G322A-mutated PSMB5 reduces bortezomib-induced apoptosis through the prevention of ubiquitinated protein accumulation and fatal ER stress in MM cell

To investigate the role of the *PSMB5* mutation (G322A) in bortezomib resistance of the MM cell lines, we transfected a G322A-mutated *PSMB5* expression construct into KMS-11 cells using a lentiviral vector. As controls, wild-type *PSMB5* or *lacZ* constructs were similarly transfected into KMS-11 cells. In Figure 3a, these transfected cells can be seen to have similar expression levels of V5-tag, which indicates that the transfection efficiency was essentially the same for the mutated *PSMB5* and the other genes. After 72-h bortezomib treatment, KMS-11 mPSMB5-V5 cells showed significant reduction of apoptosis compared with KMS-11- wPSMB5-V5-, KMS-11 lacZ-V5-transfected and nontransfected KMS-11 cells (Figure 3b). Similar result was shown in growth inhibition assay when treated with various concentrations of bortezomib for 72 h. The IC_{50} values were 8.88, 26.38, 8.83 and 113.63 nM in KMS-11 wPSMB5-V5, KMS-11 mPSMB5-V5, parental KMS-11 and KMS-11/BTZ cells, respectively (Figure 3c). There was much less accumulation of polyubiquitinated proteins in mPSMB5-transfected cells compared with wild-type control cells (Figure 3d). Similarly, expression levels of CHOP and Noxa were lower in mutated PSMB5-transfected KMS-11 cells after bortezomib exposure (Figure 3d). These results indicate that G322A-mutated *PSMB5* contributed to a reduction in bortezomib-induced apoptosis by preventing ubiquitinated protein accumulation and fatal ER stress in these MM cells.

Discussion

We have established two novel bortezomib-resistant MM cell lines, KMS-11/BTZ and OPM-2/BTZ, both of which tolerated the drug even at high concentrations and were also resistant to a different proteasome inhibitor, MG132. These two bortezomib-resistant MM cell lines did not overexpress the $\beta 5$ proteasome subunit compared with the parental lines, unlike what has been reported in bortezomib-resistant cells other than MM cells.^{16,17} However, a unique point mutation, G322A, was identified in the *PSMB5* gene as has also been found in previous studies of bortezomib-resistant cells of other hematopoietic lineages.^{16,17} In addition, we demonstrated that the G322A point mutation in *PSMB5* actually contributes to resistance against bortezomib-induced apoptosis, which is mediated by prevention of polyubiquitinated protein accumulation and fatal ER stress signaling followed by the downregulation of BH3-only protein, that is, Noxa expression. However, the degree of bortezomib resistance in mutated PSMB5-transfected KMS-11 cells was not as great as that of KMS-11/BTZ cells, indicating that as-yet unidentified mechanisms other than *PSMB5* mutation may partly contribute to the bortezomib resistance in KMS-11/BTZ cells.

A point mutation of the *PSMB5* gene (G322A) identified in both bortezomib-resistant MM cell lines results in replacement of the codon 49 Thr for Ala at the amino-acid level. This would

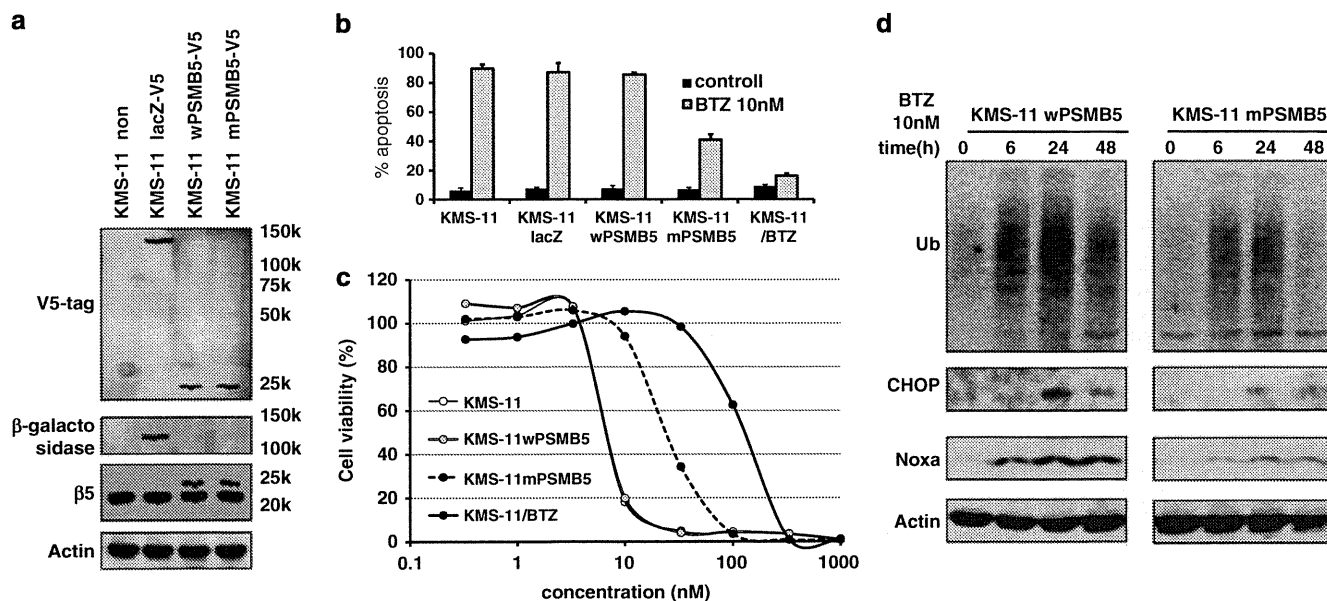


Figure 3 Comparison of bortezomib-induced apoptosis, accumulation of polyubiquitinated proteins, and the expression of CHOP between mutated PSMB5-expressing KMS-11 and wild-type PSMB5-expressing KMS-11 cells. (a) The expression of V5-tagged lacZ, V5-tagged wild-type (w) PSMB5 and V5-tagged mutated(m) PSMB5 in transfected KMS-11 cells. (b) Comparison of bortezomib-induced apoptosis at 72 h in mutated PSMB5-, wild-type PSMB5-, lacZ-, non-transfected KMS-11 cells and bortezomib-resistant cell (KMS-11/BTZ). Apoptotic cells were evaluated as Annexin V-positive cells. (c) Cell viability of mutated PSMB5-, wild-type PSMB5-, non-transfected KMS-11 cells and bortezomib-resistant KMS-11 cells (KMS-11/BTZ) after exposure to various concentrations of bortezomib for 72 h. (d) The time-dependent alteration of accumulated polyubiquitinated proteins, CHOP and Noxa expression in mutated PSMB5- and wild-type PSMB5-transfected KMS-11 cells in the presence of 10 nM bortezomib.

give rise to a conformational change of the bortezomib-binding pocket in the $\beta 5$ subunit, resulting in the partial disruption of contact between bortezomib and the chymotrypsin-like active site.^{16,21} Our study first proved that in MM cells, the G322A point mutation in PSMB5 contributes to resistance against bortezomib-induced apoptosis. Moreover, our study does not support the notion that overexpression of wild-type PSMB5 alone led to bortezomib resistance, unlike previous reports using a bortezomib-adapted monocytic/macrophage cell line.¹⁷ Among various hematological malignant cell types, MM cells have the greatest sensitivity to bortezomib even at low doses, probably due to preexisting ER overload. Thus, moderately upregulated PSMB5 may not be able to impart the resistance against bortezomib. In fact, as the mutated PSMB5 is not overexpressed in either of the bortezomib-resistant MM cell lines, the presence of this mutated form may have a major role in acquired resistance against bortezomib. Although bortezomib is a highly selective inhibitor of the chymotrypsin-like activity of PSMB5, another proteasome catalytic site, PSMB1, is also inhibited to some extent by bortezomib. Another subunit, PSMB6, is known to act as a scaffold to stabilize the interaction between bortezomib and the active site of PSMB5.²¹ However, we could not find any mutations in *PSMB1* and *PSMB6* in our bortezomib-resistant MM cells (data not shown).

We have not found any *PSMB5* gene mutations in a small number ($n=4$) of clinically available specimens derived from MM patients who showed resistance against bortezomib so far. However, further investigations using a larger number of patients who have acquired bortezomib resistance during or after treatment are required.

In conclusion, we have established two different stable bortezomib-resistant MM cell lines, both of which were found to have acquired exactly the same point mutation (G322A) in the bortezomib-binding pocket of *PSMB5*. These cells, unlike their parental cells, did not accumulate misfolded proteins and

thus avoided the catastrophic ER stress, which triggers CHOP expression and caspase-4 and -12 activations. Apoptosis triggered by Noxa induction was also suppressed. These cell lines will provide tools for the better understanding of the underlying mechanisms of bortezomib resistance, and may lead to the development of novel treatment strategies for overcoming bortezomib resistance in patients with MM.

Conflict of interest

TN, HM and YS are employees of Kyowa Hakko Kirin Co., Ltd., Japan. SI received research funding from Kyowa Hakko Kirin. SI declares honoraria from Janssen Pharmaceutical K.K., Dainippon Sumitomo Pharmaceutical Co., Ltd, Chugai Pharmaceutical Co., Ltd and Novartis Pharma K.K.

Acknowledgements

We thank Ms Chiori Fukuyama for her skillful technical assistance. This work was supported by Grants-in-Aid for Scientific Research on Priority Areas (No. 17016065 & 16062101 for RU) from the Ministry of Education, Culture, Science, Sports and Technology, Japan; and Grants-in-Aid for Cancer Research from the Ministry of Health, Labor and Welfare, Japan (No. 17S-1, 17-16 and 21-8-5 for SI). This research was also funded in part by Kyowa Hakko Kirin Co., Ltd, Tokyo, Japan.

References

- Richardson PG, Sonneveld P, Schuster MW, Irwin D, Stadtmauer EA, Facon T *et al*. Bortezomib or high-dose dexamethasone for relapsed multiple myeloma. *N Engl J Med* 2005; **352**: 2487–2498.
- San Miguel JF, Schlag R, Khuageva NK, Dimopoulos MA, Shpilberg O, Kropff M *et al*. Bortezomib plus melphalan and

- prednisone for initial treatment of multiple myeloma. *N Engl J Med* 2008; **359**: 906–917.
- 3 Kumar S, Rajkumar SV. Many facets of bortezomib resistance/susceptibility. *Blood* 2008; **112**: 2177–2178.
 - 4 Shah JJ, Orlowski RZ. Proteasome inhibitors in the treatment of multiple myeloma. *Leukemia* 2009; **23**: 1964–1979.
 - 5 Karin M, Greten FR. NF-kappaB: linking inflammation and immunity to cancer development and progression. *Nat Rev Immunol* 2005; **5**: 749–759.
 - 6 Fennell DA, Chacko A, Mutti L. BCL-2 family regulation by the 20S proteasome inhibitor bortezomib. *Oncogene* 2008; **27**: 1189–1197.
 - 7 Perez-Galan P, Roue G, Villamor N, Montserrat E, Campo E, Colomer D. The proteasome inhibitor bortezomib induces apoptosis in mantle-cell lymphoma through generation of ROS and Noxa activation independent of p53 status. *Blood* 2006; **107**: 257–264.
 - 8 Ri M, Iida S, Ishida T, Ito A, Yano H, Inagaki A *et al*. Bortezomib-induced apoptosis in mature T-cell lymphoma cells partially depends on upregulation of Noxa and functional repression of Mcl-1. *Cancer Sci* 2009; **100**: 341–348.
 - 9 Zhu H, Zhang L, Dong F, Guo W, Wu S, Teraishi F *et al*. Bik/NBK accumulation correlates with apoptosis-induction by bortezomib (PS-341, Velcade) and other proteasome inhibitors. *Oncogene* 2005; **24**: 4993–4999.
 - 10 Nawrocki ST, Carew JS, Pino MS, Highshaw RA, Dunner Jr K, Huang P *et al*. Bortezomib sensitizes pancreatic cancer cells to endoplasmic reticulum stress-mediated apoptosis. *Cancer Res* 2005; **65**: 11658–11666.
 - 11 Obeng EA, Carlson LM, Gutman DM, Harrington Jr WJ, Lee KP, Boise LH. Proteasome inhibitors induce a terminal unfolded protein response in multiple myeloma cells. *Blood* 2006; **107**: 4907–4916.
 - 12 Adams J. The development of proteasome inhibitors as anticancer drugs. *Cancer Cell* 2004; **5**: 417–421.
 - 13 Schroder M, Kaufman RJ. The mammalian unfolded protein response. *Annu Rev Biochem* 2005; **74**: 739–789.
 - 14 Yoshida H. ER stress and diseases. *FEBS J* 2007; **274**: 630–658.
 - 15 Moenner M, Pluquet O, Bouche-careilh M, Chevet E. Integrated endoplasmic reticulum stress responses in cancer. *Cancer Res* 2007; **67**: 10631–10634.
 - 16 Lu S, Yang J, Song X, Gong S, Zhou H, Guo L *et al*. Point mutation of the proteasome beta5 subunit gene is an important mechanism of bortezomib resistance in bortezomib-selected variants of Jurkat T cell lymphoblastic lymphoma/leukemia line. *J Pharmacol Exp Ther* 2008; **326**: 423–431.
 - 17 Oerlemans R, Franke NE, Assaraf YG, Cloos J, van Zantwijk I, Berkers CR *et al*. Molecular basis of bortezomib resistance: proteasome subunit beta5 (PSMB5) gene mutation and over-expression of PSMB5 protein. *Blood* 2008; **112**: 2489–2499.
 - 18 Ruckrich T, Kraus M, Gogel J, Beck A, Ovaa H, Verdoes M *et al*. Characterization of the ubiquitin-proteasome system in bortezomib-adapted cells. *Leukemia* 2009; **23**: 1098–1105.
 - 19 Wang Q, Mora-Jensen H, Weniger MA, Perez-Galan P, Wolford C, Hai T *et al*. ERAD inhibitors integrate ER stress with an epigenetic mechanism to activate BH3-only protein NOXA in cancer cells. *Proc Natl Acad Sci USA* 2009; **106**: 2200–2205.
 - 20 Hideshima T, Ikeda H, Chauhan D, Okawa Y, Raje N, Podar K *et al*. Bortezomib induces canonical nuclear factor-kappaB activation in multiple myeloma cells. *Blood* 2009; **114**: 1046–1052.
 - 21 Groll M, Berkers CR, Ploegh HL, Ovaa H. Crystal structure of the boronic acid-based proteasome inhibitor bortezomib in complex with the yeast 20S proteasome. *Structure* 2006; **14**: 451–456.

Supplementary Information accompanies the paper on the Leukemia website (<http://www.nature.com/leu>)

Schwann cell autophagy induced by SAHA, 17-AAG, or clonazepam can reduce bortezomib-induced peripheral neuropathy

T Watanabe^{*,1}, K Nagase¹, M Chosa¹ and K Tobinai¹

¹Hematology Division, National Cancer Center Hospital, 5-1-1 Tsukiji, Chuo-ku, Tokyo 104-0045, Japan

BACKGROUND: The proteasome inhibitor bortezomib has improved the survival of patients with multiple myeloma but bortezomib-induced peripheral neuropathy (BiPN) has emerged as a serious potential complication of this therapy. Animal studies suggest that bortezomib predominantly causes pathological changes in Schwann cells. A tractable system to evaluate combination drugs for use with bortezomib is essential to enable continuing clinical benefit from this drug.

METHODS: Rat schwannoma cells were pretreated with vincristine (VCR), histone deacetylase inhibitors, anticonvulsants, or a heat-shock protein 90 (HSP90) inhibitor. To then monitor aggresome formation as a result of proteasome inhibition and the activation of chaperone-mediated autophagy (CMA), we performed double-labelling immunofluorescent analyses of a cellular aggregation-prone protein marker.

RESULTS: Aggresome formation was interrupted by VCR, whereas combination treatments with bortezomib involving suberoylanilide hydroxamic acid, 17-allylamino-17-demethoxy-geldanamycin, or clonazepam appear to facilitate the disposal of unfolded proteins via CMA, inducing HSP70 and lysosome-associated membrane protein type 2A (LAMP-2A).

CONCLUSIONS: This schwannoma model can be used to test BiPN-reducing drugs. The present data suggest that aggresome formation in Schwann cells is a possible mechanism of BiPN, and drugs that induce HSP70 or LAMP-2A have the potential to alleviate this complication. Combination clinical trials are warranted to confirm the relevance of these observations.

British Journal of Cancer (2010) **103**, 1580–1587. doi:10.1038/sj.bjc.6605954 www.bjcancer.com

Published online 19 October 2010

© 2010 Cancer Research UK

Keywords: autophagy; multiple myeloma; neuropathy; proteasome inhibitors

The development of novel agents, such as proteasome inhibitors and immunomodulatory drugs has improved the survival outcome for multiple myeloma (MM) patients (Kumar *et al*, 2008). However, the incidence of peripheral neuropathy (PN) has emerged as a significant problem in the new therapeutic era for MM (Richardson *et al*, 2006, 2009b; Argyriou *et al*, 2008). In younger patients with MM, primary treatments have included vincristine (VCR), doxorubicin, and dexamethasone, and also high-dose therapy with melphalan supported by autologous stem cell transplantation. However, in some of these patients, VCR treatments have caused PN. Moreover, bortezomib was the first proteasome inhibitor to be approved for the treatment of relapsed/refractory as well as newly diagnosed MM patients (Richardson *et al*, 2003; San Miguel *et al*, 2008). However, this treatment can cause peripheral nerve damage leading to the development of bortezomib-induced peripheral neuropathy (BiPN). Owing to these adverse effect, bortezomib will be discontinued even in patients that respond well to this drug. Not surprisingly, bortezomib has recently become one of the mainstays in ongoing clinical trials of combination therapies for MM.

A couple of recent studies have reported neurophysiological and pathological findings for bortezomib administration in animal models (Cavaletti *et al*, 2007; Bruna *et al*, 2010; Merregalli *et al*, 2010). Another histopathological study in rats reported that bortezomib did not affect neurons but did cause damage to Schwann cells (Cavaletti *et al*, 2007). Another report has however shown that alterations to Schwann cells might be a secondary effect of bortezomib (Bruna *et al*, 2010). At present, treatments for BiPN are lacking, although anticonvulsants have been administered to MM patients with this disorder (Richardson *et al*, 2006; Argyriou *et al*, 2008). In addition, although a dose-modification guideline for BiPN has been published (Richardson *et al*, 2009b), it is difficult to accurately evaluate neurotoxicity in patients during bortezomib therapy and thus determine when treatment should discontinue. Hence, combination bortezomib treatments for MM involving agents that function as prophylactics against BiPN, rather than drugs that treat BiPN, are highly desirable. However, there are currently few (if any) investigative tools available to develop such therapies as the molecular mechanisms underlying BiPN remain to be elucidated.

To elucidate the molecular mechanisms underpinning the onset of BiPN in our current study, we first reviewed previous reports on neurodegenerative diseases in which protein aggregates are responsible for the cellular toxicity. When the activity of proteasome is inhibited, misfolded proteins will form aggregates

*Correspondence: Dr T Watanabe; E-mail: takawata@ncc.go.jp
Revised 10 September 2010; accepted 21 September 2010; published online 19 October 2010

known as aggresomes (Johnston *et al*, 1998). Aggresomes were initially described as inclusion bodies in the cells of patients with neurodegenerative diseases (Kopito, 2000) such as amyotrophic lateral sclerosis (Bruijn *et al*, 1998; Mezey *et al*, 1998), Parkinson's disease (Mezey *et al*, 1998), and Huntington's disease (Bennett *et al*, 2007). In our present experiments, we employed a schwannoma cell system to monitor aggresome formation after treatment with bortezomib. Furthermore, we examined whether additional treatments could reduce the number and size of these aggregates and thus potentially suppress the onset of BiPN.

MATERIALS AND METHODS

Schwann cell pretreatment and bortezomib treatment

A rat schwannoma cell line RT4-D6P2T (purchased from ATCC, Manassas, VA, USA, on 28 May 2007) was cultured in Dulbecco's modified Eagle's medium (Sigma-Aldrich, St Louis, MO, USA) containing 10% FBS (Bioserum, Victoria, Australia). RT4-D6P2T cells were cultured for less than 2 months after reconstitution from stocks, which were frozen upon receipt from the ATCC. The cells

had been validated by the supplier using DNA fingerprinting and no additional authentication was performed in our laboratory. The morphology of the RT4-D6P2T cells showed no changes over the course of the study.

At 1 day before pretreatment, the RT4-D6P2T cells were plated at a density of 5×10^4 cells per well on four-well chamber slides. They were then either untreated or pretreated with 40 nM VCR (Sigma-Aldrich) for 1 h or pretreated for 24 h with either 5 μ M suberoylanilide hydroxamic acid (SAHA; Merck & Co. Inc., Whitehouse Station, NJ, USA), 0.5 μ M 17-allylamino-17-demethoxy-geldanamycin (17-AAG; Sigma-Aldrich), 50 nM clonazepam (CZP; Sigma-Aldrich), or 6 mM valproic acid (VPA; Sigma-Aldrich). The dose of each reagent was determined by its half maximal inhibitory value (IC_{50}). For VCR pretreatments, the cells were washed twice with PBS: 2.68 mM KCl, 1.47 mM KH_2PO_4 , 136.89 mM NaCl, and 8.10 mM Na_2HPO_4 (Dainippon Sumitomo Pharma Co. Ltd., Osaka, Japan) before the addition of 40 nM bortezomib (Millennium Pharmaceuticals, Cambridge, MA, USA) for 3 h. Following pretreatment with other reagents, the cells were not washed before the 3-h treatment with 40 nM bortezomib. As a final step, the cells were washed twice with PBS, incubated for a further 24 h, and then fixed.

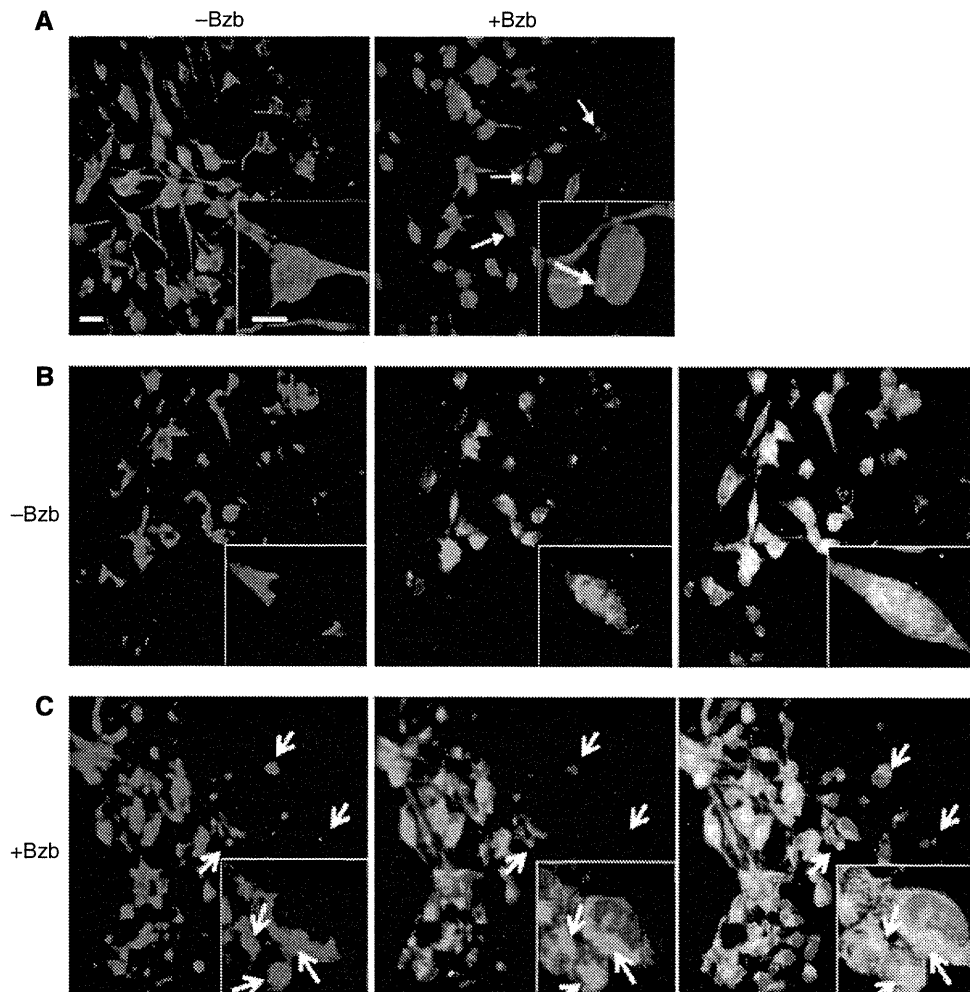


Figure 1 Bortezomib induces aggresome formation at the microtubule-organising centres (MTOCs) of Schwann cells. **(A)** In untreated RT4-D6P2T cells, γ -tubulin is distributed homogeneously throughout the cytoplasm (left panel). In bortezomib (Bzb)-treated cells, aggresomes form as distinct pericentriolar structures (arrows) with weak staining in the cytoplasm (right panel). Insets in the right panel show the juxtannuclear rounded structures evident at higher magnification. **(B)** Untreated RT4-D6P2T cells contain dynein (red), which is distributed homogeneously in the cytoplasm with predominant localisation in the perinuclear region, and vimentin (green), which is distributed diffusely throughout the cytoplasm and above the nuclei. **(C)** In bortezomib-treated cells, dynein (red) and vimentin (green) appear as rounded structures at the MTOC (arrows) and are colocalised in the region adjacent to the nuclei (yellow signals in the merged image of both fluorochrome channels). Bar, 20 μ m. -Bzb, untreated; +Bzb, bortezomib treated.

Immunohistochemical analysis

The RT4-D6P2T cells were fixed with PBS containing 4% paraformaldehyde for 10 min at 4°C, washed with TBS (20 mM Tris and 500 mM NaCl (pH 7.4)) with 0.1% IGEPAL CA-630 (Fluka, Buchs, Switzerland) for 3 × 5 min, fixed in methanol for 10 min at 4°C, and blocked with PBS containing 4% BSA (Sigma-Aldrich) for 30 min at room temperature. The cells were then incubated overnight at 4°C with primary antibodies diluted at a ratio of 1:50 in PBS with 4% BSA (γ -tubulin (Sigma-Aldrich), dynein (Sigma-Aldrich), vimentin (Santa Cruz Biotechnology, Santa Cruz, CA, USA), heat-shock protein 70 (HSP70; Santa Cruz Biotechnology), peripheral myelin protein 22 (PMP22; Millipore, Bedford, MA, USA), and lysosome-associated membrane protein type 2A (LAMP-2A; Abcam, Cambridge, MA, USA)). The cells were then washed 3 × 5 min in TBS with 0.1% IGEPAL CA-630 and incubated with secondary antibodies diluted at a ratio of 1:100 in PBS with

4% BSA, for 1 h at room temperature (Alexa Fluor 488-conjugated chicken anti-rabbit IgG and Alexa Fluor 555-conjugated goat anti-mouse IgG (Molecular Probes, Eugene, OR, USA)). After a further washing for 3 × 5 min in TBS with 0.1% IGEPAL CA-630, the cells were mounted on slides with VECTASHIELD (Vector Laboratories, Burlingame, CA, USA). We note that all washes were performed at room temperature. Images of the cells were captured on a laser scanning confocal microscope BZ-8000 (Keyence, Osaka, Japan) and analysed by BZ-Analyzer software (Keyence). The thickness of the optical sections analysed was 0.4 μ m.

Quantification of aggresomes and round structures outside of the Schwann cells

Aggresomes and round structures outside of the cells were identified by the colocalisation of PMP22 and γ -tubulin, counted

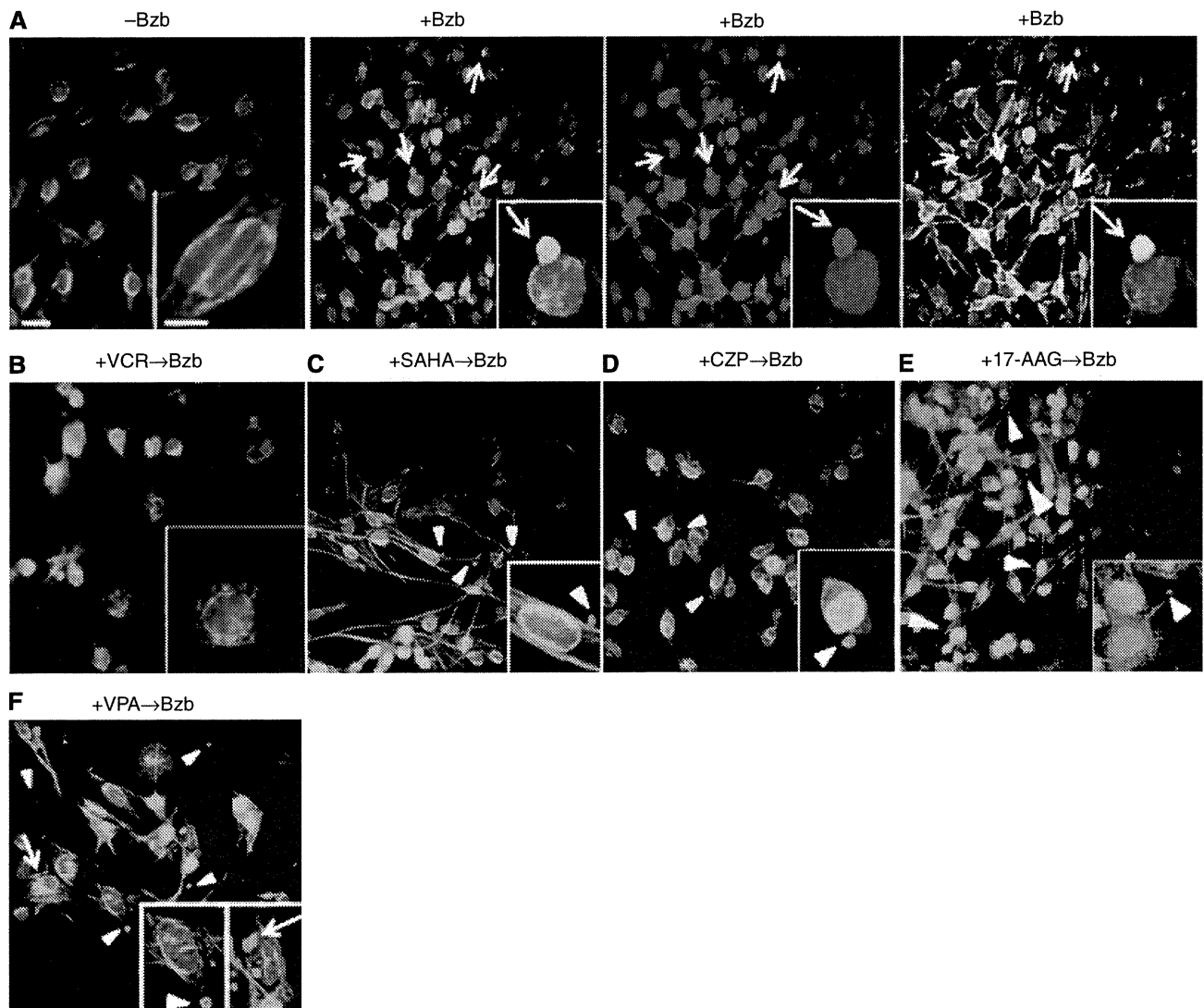


Figure 2 Vincristine (VCR) abrogates aggresome formation and in a combination treatment with bortezomib augments the exocytosis of endogenous misfolded proteins. **(A)** Peripheral myelin protein 22 (PMP22) is homogeneously distributed throughout the cytoplasm of RT4-D6P2T cells before treatment with bortezomib (left panel). After treatment with bortezomib (Bzb), PMP22 appears to undergo retrograde transport towards the MTOC where it forms perinuclear aggresomes (arrows, middle panel, green signals) and colocalises with γ -tubulin (arrows, middle panel, red signals). A merged image of both fluorophores is shown in the far right panel (yellow signal). **(B)** Following pretreatment with VCR, a microtubule depolymerisation agent, PMP22 signals are evident at multiple sites in a granular pattern of aggregates throughout the cytoplasm, most notably in the perikaryon. Cells pretreated with **(C)** suberoylanilide hydroxamic acid (SAHA), a known histone deacetylase inhibitor (HDACi), or **(D)** clonazepam (CZP), an anticonvulsant, and **(E)** 17-allylamino-17-demethoxy-geldanamycin (17-AAG), a HSP90 inhibitor, fail to form aggresomes, but instead form rounded structures outside of the cell (arrowheads), which are smaller than the perinuclear aggresomes. **(F)** Pretreatment with valproic acid (VPA) causes the appearance of similar rounded structures outside of the cells (arrowheads) in addition to juxtannuclear aggresomes (arrows).

in triplicate from 200 cells, and expressed as a percentage of the total cells.

Growth inhibition assay of MM cells

The human MM cell lines, MM.1S, RPMI8226 (purchased from ATCC), and KMS-18 (kindly provided by Dr T Otsuki, Department of Hygiene, Kawasaki Medical School, Kurashiki, Japan) were maintained in RPMI1640 (Sigma-Aldrich) containing 10% FBS. The growth-inhibitory effects upon MM cells were determined using a 3-(4, 5-dimethyl-2-thiazolyl)-2,5-diphenyl-2H-tetrazolium bromide (MTT) assay (Sigma-Aldrich). At 1 day before treatment, 9.0×10^4 cells per 90 μ l aliquot were cultured in 96-well plates (Sumitomo Bakelite, Higashikangawa, Japan) in triplicate at 37°C. Cells were either untreated or pretreated for 24 h with the same concentration of each reagent used with the RT4-D6P2T cells except for VCR. The cells were then cultured further with varying concentrations (from 0.5 to 3 nM) of bortezomib for 48 h. Optical densities (ODs) at 570 and 630 nm were measured using a multiplate reader. Stock MTT was added to each of the wells in the assay, and the plates were further incubated at 37°C for 5 h. Dimethyl sulphoxide (Sigma-Aldrich) was added to all wells and mixed thoroughly. After a few minutes at room temperature to ensure that all formazan crystals were dissolved, the plates were read on a SpectroMax 340PC³⁸⁴ VersaMax (Molecular Devices, Sunnyvale, CA, USA), using a test wavelength of 570 nm and a reference wavelength of 630 nm. Cell growth (%) was calculated as follows: $(OD_{630} - OD_{570} \text{ of the samples} / OD_{630} - OD_{570} \text{ of the control}) \times 100$.

RESULTS

Aggresomes form at MTOC following proteasome inhibition in Schwann cells

A diffuse expression pattern of γ -tubulin, a protein that adheres to the centrosome (Dichtenberg *et al*, 1998), was observed in the cytoplasm of RT4-D6P2T cells. Following a 3-h treatment with 40 nM bortezomib, however, γ -tubulin staining in the cytoplasm became weak and coalesced to form round structures in the juxtannuclear area (Figure 1A). Similarly, the dynein and vimentin proteins became rounded and colocalised in region adjacent to the nucleus after exposure to bortezomib (Figure 1C).

Vincristine abrogates bortezomib-induced aggresome formation and combination treatments augment the exocytosis of endogenous misfolded proteins from Schwann cells

We next examined whether endogenous misfolded proteins destined to be processed by the ubiquitin-proteasome system could be induced to aggregate and undergo retrograde transport towards the microtubule-organising center (MTOC) upon proteasome inhibition. To accomplish this, we employed the cellular marker PMP22, a short-lived glycoprotein present in Schwann cells (Fortun *et al*, 2003). Following bortezomib treatment, PMP22 showed a distinct juxtannuclear and rounded appearance and colocalised with γ -tubulin to form aggresomes (Figure 2A), as previously reported (Fortun *et al*, 2003). Interestingly, treatments with VCR completely abrogated the bortezomib-induced accumulation of PMP22, which was instead observed as numerous spots in the perikaryon (Figure 2B).

We next analysed whether treatments with a combination of reagents could reduce aggresome formation. Intriguingly, pretreatment with the histone deacetylase inhibitor (HDACi) SAHA (Figure 2C), the anticonvulsant CZP (Figure 2D), or the HSP90 inhibitor 17-AAG (Figure 2E) caused the appearance of round structures, which were smaller than aggresomes, outside of the

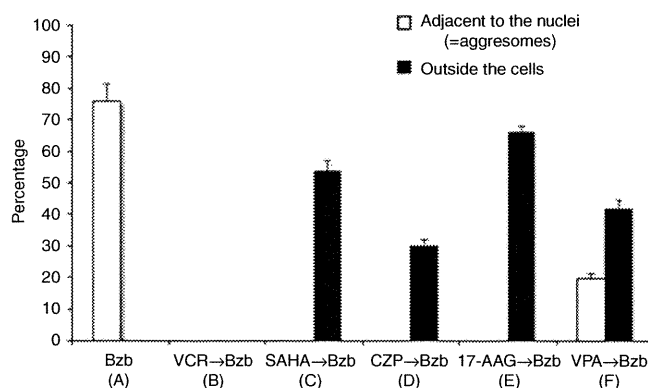


Figure 3 The percentages of round structures adjacent to the nuclei (i.e., aggresomes) and outside the cells were calculated from images showing the colocalisation of PMP22 and γ -tubulin (yellow signals in the far right panel in Figure 2A). These numbers were measured in triplicate and are expressed as the means \pm s.d. The letters in parentheses under the treatment categories correspond to the images above.

cells and with no juxtannuclear aggresomes (Figure 3). In contrast, pretreatment with VPA, also an anticonvulsant and an HDACi, caused the appearance of rounded structures outside of the cells in addition to juxtannuclear aggresomes (Figures 2F and 3).

Chaperone-mediated autophagy is responsible for the enhanced exocytosis of misfolded proteins in Schwann cells during proteasome inhibition

To analyse the molecular mechanisms underlying the enhanced exocytosis of misfolded proteins in Schwann cells, we used an antibodies against the HSP70 chaperone protein and the receptor for chaperone-mediated autophagy (CMA) at the lysosomal membrane (which is a unique isoform of LAMP-2, LAMP-2A) (Cuervo and Dice, 2000; Kaushik *et al*, 2006). After treatment with SAHA, 17-AAG, or CZP (Figure 4A, B, or C, respectively) followed by bortezomib, HSP70 and LAMP-2A were found to colocalise in structures outside of the cells.

Drugs that protect Schwann cells from aggresome formation due to bortezomib treatment do not disrupt the growth inhibitory effects of bortezomib in myeloma cells

Pretreatments of MM cells with the same drugs used in the RT4-D6P2T cell experiments had few negative effects on the profound growth inhibitory effects of bortezomib (Figure 5).

DISCUSSION

The findings of our present study using a schwannoma cell model system suggest that aggresome formations caused by proteasome inhibition and the excretion pathways of intracellular misfolded proteins are targets for combination drug candidates that will alleviate the onset of BiPN during bortezomib treatment.

A recent study of skin biopsies has revealed that BiPN manifests as predominantly large fibres (Chaudhry *et al*, 2008). On the other hand, in some BiPN patients who develop treatment-emergent neuropathy, the underlying cause has been attributed to the impairment of small fibres (Richardson *et al*, 2006), even though such fibres comprise myelinated A δ and unmyelinated C fibres. In contrast, it has been proposed that 68–85% of BiPN cases are reversible (Richardson *et al*, 2009a, b).

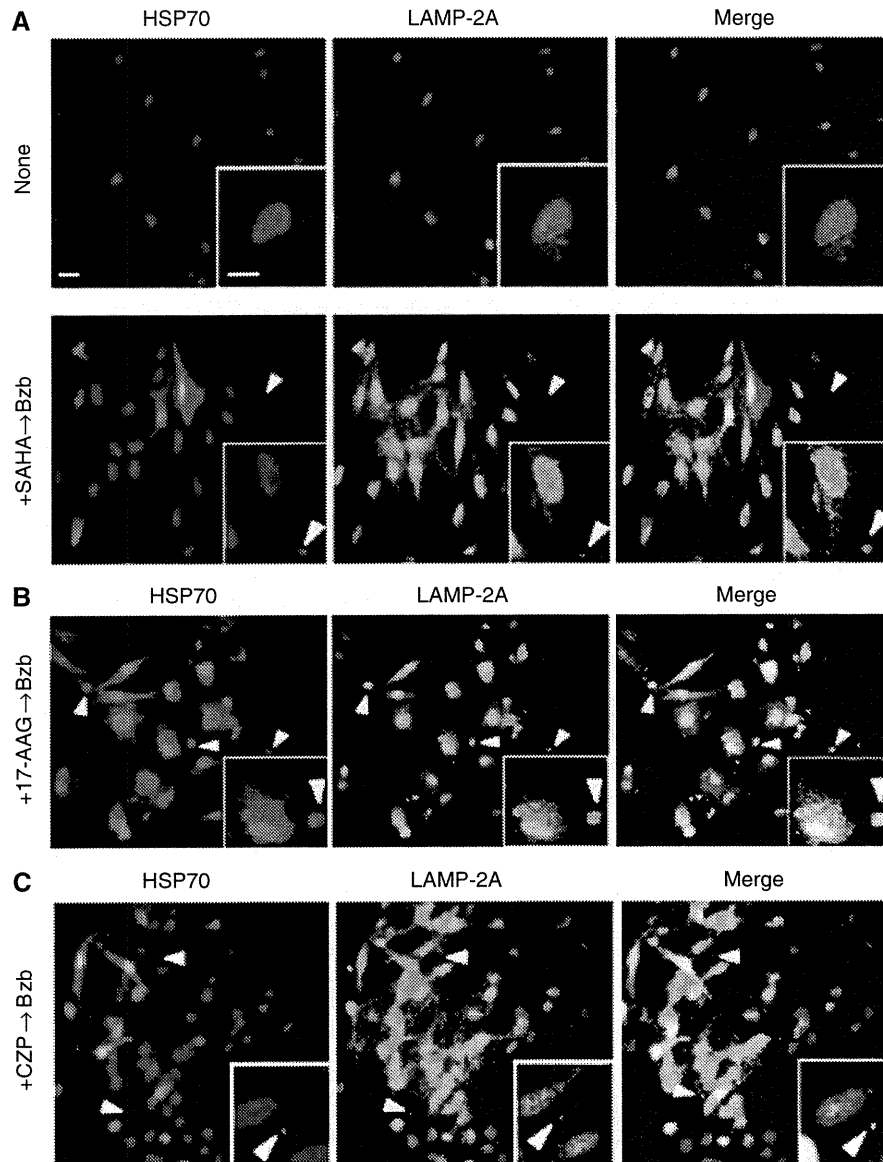


Figure 4 Combination treatments with bortezomib can augment the exocytosis of misfolded proteins through the chaperone-mediated autophagy of Schwann cells. The distributions of HSP70/HSC70 (red), a chaperone protein, and LAMP-2A (green), a lysosomal membrane protein with a specific role in chaperone-mediated autophagy, are shown in response to combination treatments with (A) SAHA, (B) 17-AAG, and (C) CZP. The colocalisation of both proteins is evidenced by the small rounded structures outside of the cells that appear as an orange signal (arrowheads). Bar, 20 μ m.

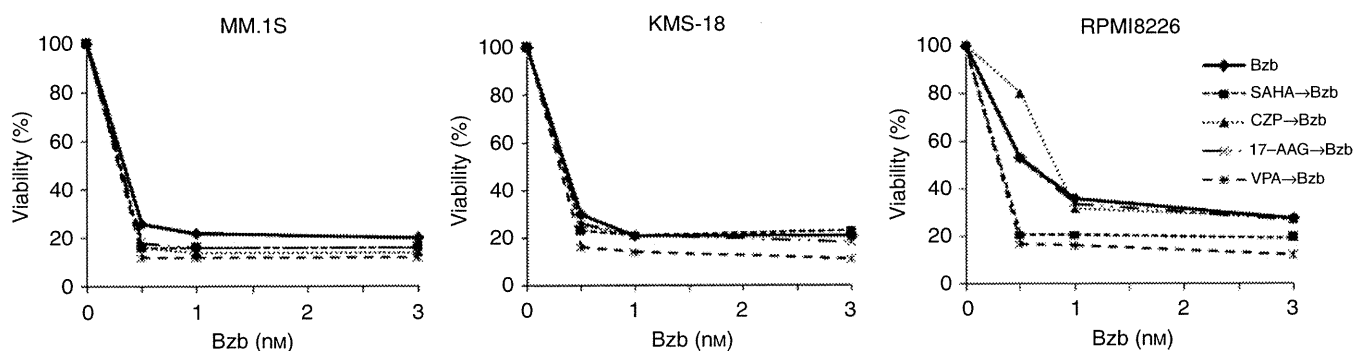


Figure 5 The same combinations used in Figures 2 and 3 do not suppress the growth inhibition of multiple myeloma (MM) cells induced by bortezomib. In MM, cells (MM.1S, KMS-18, and RPMI8226) were treated with bortezomib alone or in combination with SAHA, CZP, 17-AAG, or VPA. The proportion of viable cells after pretreatment with each drug followed by bortezomib treatment is indicated as a percentage of the untreated cells. These numbers were measured in triplicate and are expressed as the means \pm s.d.

Although it has already been demonstrated that the behaviour of cells of neoplastic origin can differ markedly from normal cells (Scuteri *et al*, 2006), cell lines are usually more tractable for experimental purpose than primary culture cells. In addition, because BiPN is predominantly sensory (Richardson *et al*, 2006; Richardson *et al*, 2009a, b), it would have been desirable to use cell

lines that would somewhat mimic the peripheral sensory nerves. No such cells are currently available however and we thus employed schwannoma cells for analysis, which are benign and differentiated tumour cells, rather than neuroblastoma cells used in previous reports (Scuteri *et al*, 2006; Csizmadia *et al*, 2008).

Our present data are consistent with previous observations that misfolded proteins form aggregates throughout the cell if they are not degraded by the proteasome (Figure 2B). Furthermore, such aggregates are then transported in a microtubule (MT)-dependent manner to the MTOC on the dynein motor complex (Figure 1C, red) (Johnston *et al*, 1998; Kopito, 2000; Garcia-Mata *et al*, 2002). After treatment with bortezomib, it has been shown that vimentin, the most common component of the intermediate filament cytoskeleton (Franke *et al*, 1978), collapses to form a 'cage' surrounding the aggresome, which then adopts a 'rounded' morphology (Figure 1C, green) (Johnston *et al*, 1998; Garcia-Mata *et al*, 1999). Moreover, our observations of aggresome formations with a distinct juxtannuclear spherical appearance that colocalise with γ -tubulin (Figure 1A, right) after treatment with proteasome inhibitor in Schwann cells corroborate those of a previous study (Fortun *et al*, 2003). Moreover, our results demonstrating that the fate of intracellular ubiquitinated aggregation-prone proteins may be relevant to the development of BiPN support previous findings for the gene expression profiles of bone marrow cells in MM patients with treatment-emergent BiPN (Richardson *et al*, 2009b). These authors identified distinct classes of gene transcripts, namely those involved in the initiation and regulation of protein translation, and their results indicated that enriched proteins that are released from MM cells may be toxic to the peripheral nervous system (Richardson *et al*, 2009b).

PMP22 is associated with a demyelinating PN, Charcot-Marie-Tooth disease type 1A (Patel *et al*, 1992), and VCR is contra-indicated in patients with this disease. In our present study, we observed that VCR treatment resulted in the dispersion of aggregates in the cytoplasm and no formation of juxtannuclear aggresomes (Figure 2B). In other words, because VCR is an MT-disrupting drug, our result suggests that pretreatment with this agent might increase BiPN by hindering the movement of unfolded proteins along the MTs with dynein motor complexes (Figure 6A). Indeed, other investigators have suggested that the neuropathy produced by VCR treatment may compromise the ability of the patients to receive bortezomib (Kyle and Rajkumar, 2009).

The central aim of our current study was to develop a clinically relevant *in vitro* system to test drugs that could be combined with bortezomib to reduce the incidence of BiPN. One of the tested candidates was the anticonvulsant VPA, which has been used previously to alleviate the symptoms of painful diabetic neuropathy (Kochar *et al*, 2004). However, the 6 mM concentration of VPA used in our experiments is more than 4000-fold higher than the previously reported clinical dosage (Munster *et al*, 2009). Furthermore, our results suggest that VPA may be less effective in

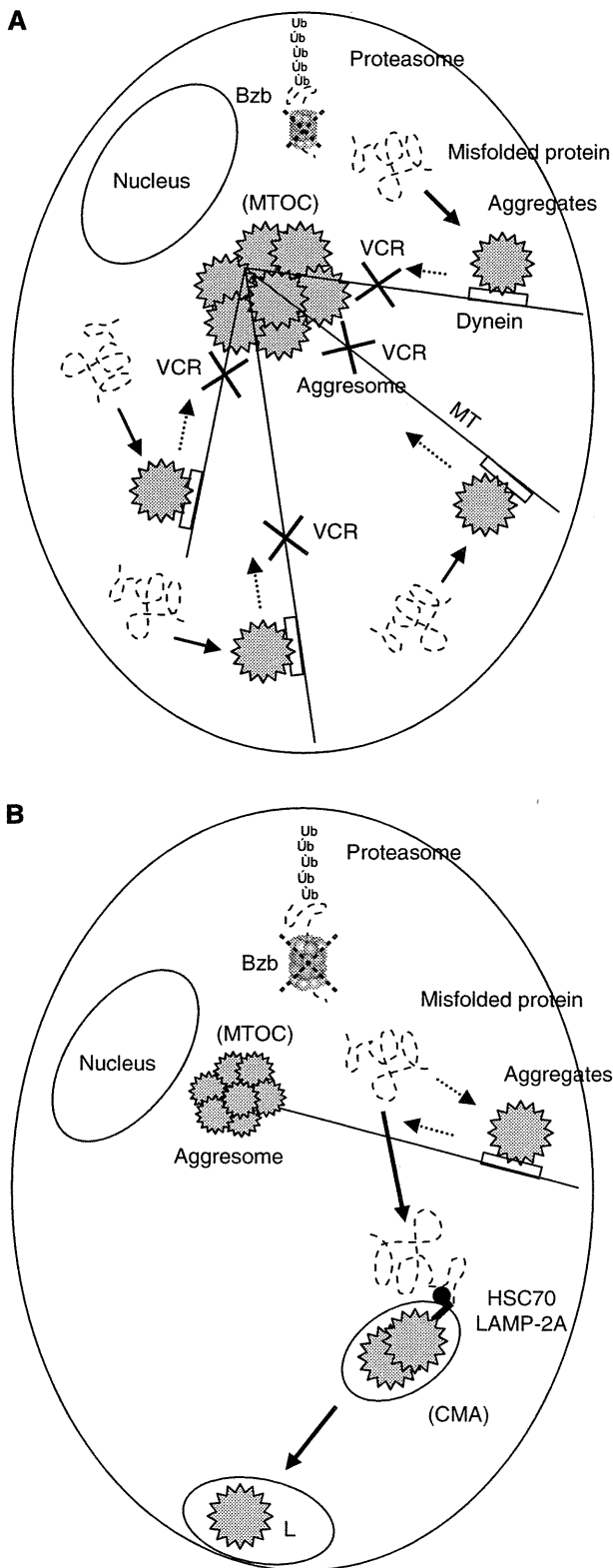


Figure 6 Schematic representation of the disruption of aggresome formation (A) and chaperone-mediated autophagy (CMA) (B). (A) Small peripherally formed aggregates are transported along the microtubule (MT) tracks by retrograde motors (i.e., dyneins) to a juxtannuclear pericentriolar location, the MT organisation centre (MTOC). 'Xvcr' indicates that VCR pretreatment before the administration of bortezomib (Bzb) hinders aggresome formation. This is likely because VCR is an MT-disrupting drug and the aggregates would be unable to move along the MTs towards the MTOC. (B) SAHA, CZP, 17-AAG, and VPA have the potential to enhance the expression of HSP70/heat-shock cognate protein of 70 Kd (HSC70), which recognises the specific motif targeted by CMA in its substrate proteins. Lysosome-associated membrane protein type 2A (LAMP-2A) is a unique receptor for CMA. Aggregated proteins are delivered from the cytoplasm out of the cells through lysosomes (L) by CMA.

reducing BiPN than other HDACi's such as SAHA or anticonvulsants like CZP. Indeed, pretreatment with VPA followed by bortezomib was found to elicit juxtannuclear aggresome formation in addition to the formation of rounded structures outside of the cells (Figures 2F and 3). On the other hand, SAHA has been shown previously to disrupt bortezomib-induced aggresome formation in MM cells (Nawrocki *et al*, 2008) as a result of the destruction of HDAC6, which promotes aggresome inclusion of misfolded polyubiquitylated proteins on the dynein motor complexes along the MTs (Kawaguchi *et al*, 2003). The 5 μM concentration of SAHA used in this study was two- to five-fold higher than the clinically usable dose in our previous pharmacokinetic analyses of phase I trials of oral SAHA (Watanabe *et al*, 2010). However, the 40 nM quantity of bortezomib used in this study is equivalent to that observed in our earlier study (Ogawa *et al*, 2008), and the 40 nM of VCR, 50 nM of CZP, and 0.5 μM of 17-AAG used in our analyses are equivalent to the doses for these compounds reported in other studies (Goetz *et al*, 2005; Corona *et al*, 2008; dos Santos *et al*, 2009, respectively).

The results of our current analyses shown in Figure 4 suggest that following pretreatment with the candidate drugs, the aggregated proteins are discarded outside of the cells by CMA (Kaushik *et al*, 2006). The evidence in support of CMA as the mechanism of disposal in this case is that the antibody used in our experiments does not distinguish between HSP70 and the heat-shock cognate protein of 70 Kd (HSC70) (Shen *et al*, 2009), which recognises the CMA-targeting motif in the substrate protein (Agarraberes *et al*, 1997). To our knowledge, the role of CMA either under conditions of proteasome inhibition or in the nervous system has never been previously reported. However, HSP70 and LAMP-2A, a specific receptor for CMA, were found in our analysis to be colocalised in the rounded structures including misfolded proteins (Figure 4). By inducing the chaperone protein, we speculate that these agents may promote an additional degradation pathway via lysosomes to excrete aggregated proteins from Schwann cells. This is different from the retrograde transport of aggregated proteins to form aggresomes along MTs from the periphery in the cytoplasm to the MTOC, thus aiding cells in the disposal of aggregated proteins (Figure 6B).

The overexpression of HSP70, which could be induced by SAHA alone in our experiments (Figure 4A, data not shown), is a

well-described consequence of HSP90 inhibition by 17-AAG (Guo *et al*, 2005). This finding is consistent with the results from series of previous reports, which showed that a pan-HDACi similar to SAHA inhibits the HSP90 deacetylase HDAC6 (Bali *et al*, 2005), and that acetylation of HSP90 releases heat-shock factor-1 from HSP90 (Zou *et al*, 1998) and consequently induces HSP70 expression (Morimoto, 1998). Furthermore, our present *in vitro* data may corroborate the results of a clinical trial with bortezomib and tanespimycin (a cremophor-based formulation of 17-AAG) in which BiPN was reduced (Mitsiades *et al*, 2009; Richardson *et al*, 2010). In the case of SAHA, a multicentre phase I trial in combination with bortezomib for relapsed or refractory MM patients has been performed and only mild PN was reported (Badros *et al*, 2009). Another case series has reported gastrointestinal tract events only without discontinuation or dose adjustments of either agent (Mazumder *et al*, 2010). Interestingly, HSP70 has also been shown to have a major role in the cellular defence against the toxic effects of misfolded proteins in neurodegenerative diseases such as amyotrophic lateral sclerosis (Gifondorwa *et al*, 2007), Parkinson's disease (Roodveldt *et al*, 2009), and Huntington's disease (Wacker *et al*, 2009).

As the binding of substrates, that is, misfolded proteins, to LAMP-2A is the limiting step for degradation via CMA (Cuervo and Dice, 1996), the induction of LAMP-2A as well as HSP70/HSC70 may be a promising marker for screening drugs that may reduce BiPN.

In summary, although the results of our present study are preliminary and *in vitro* only, our data suggest that the combination of bortezomib and SAHA, 17-AAG, or CZP has the potential to reduce BiPN. As bortezomib is currently an important component of combination treatment for MM, our *in vitro* system may allow MM patients to continue to benefit from bortezomib in the future.

ACKNOWLEDGEMENTS

This work was supported by a grant-in-aid for Cancer Research (21-8) from the Ministry of Health, Labour and Welfare of Japan (T Watanabe).

REFERENCES

- Agarraberes FA, Terlecky SR, Dice JF (1997) An intralysosomal hsp70 is required for a selective pathway of lysosomal protein degradation. *J Cell Biol* 137: 825–834
- Argyriou AA, Iconomou G, Kalofonos HP (2008) Bortezomib-induced peripheral neuropathy in multiple myeloma: a comprehensive review of the literature. *Blood* 112: 1593–1599
- Badros A, Burger AM, Philip S, Niesvizky R, Kolla SS, Goloubeva O, Harris C, Zwiebel J, Wright JJ, Espinoza-Delgado I, Baer MR, Holleran JL, Egorin MJ, Grant S (2009) Phase I study of vorinostat in combination with bortezomib for relapsed and refractory multiple myeloma. *Clin Cancer Res* 15: 5250–5257
- Bali P, Pranpat M, Bradner J, Balasis M, Fiskus W, Guo F, Rocha K, Kumaraswamy S, Boyapalle S, Atadja P, Seto E, Bhalla K (2005) Inhibition of histone deacetylase 6 acetylates and disrupts the chaperone function of heat shock protein 90: a novel basis for antileukemia activity of histone deacetylase inhibitors. *J Biol Chem* 280: 26729–26734
- Bennett EJ, Shaler TA, Woodman B, Ryu K-Y, Zaitseva TS, Becker CH, Bates GP, Schulman H, Kopito RR (2007) Global changes to the ubiquitin system in Huntington's disease. *Nature* 448: 704–708
- Brujin LI, Houseweart MK, Kato S, Anderson KL, Anderson SD, Ohama E, Reaume AG, Scott RW, Cleveland DW (1998) Aggregation and motor neuron toxicity of an ALS-linked SOD1 mutant independent from wild-type SOD1. *Science* 281: 1851–1854
- Bruna J, Udina E, Alé A, Vilches JJ, Vynckier A, Monbaliu J, Silverman L, Navarro X (2010) Neurophysiological, histological and immunohistochemical characterization of bortezomib-induced neuropathy in mice. *Exp Neurol* 223: 599–608
- Cavaletti G, Gilardini A, Canta A, Rigamonti L, Rodriguez-Menendez V, Ceresa C, Marmiroli P, Bossi M, Oggioni N, D'Incalci M, De Coster R (2007) Bortezomib-induced peripheral neurotoxicity: a neurophysiological and pathological study in the rat. *Exp Neurol* 204: 317–325
- Chaudhry V, Cornblath DR, Polydefkis M, Ferguson A, Borrello I (2008) Characteristics of bortezomib- and thalidomide-induced peripheral neuropathy. *J Peripher Nerv Syst* 13: 275–282
- Corona G, Casetta B, Sandron S, Vaccher E, Toffoli G (2008) Rapid and sensitive analysis of vincristine in human plasma using on-line extraction combined with liquid chromatography/tandem mass spectrometry. *Rapid Commun Mass Spectrom* 22: 519–525
- Csizmadia V, Raczynski A, Csizmadia E, Fedyk ER, Rottman J, Alden CL (2008) Effect of an experimental proteasome inhibitor on the cytoskeleton, cytosolic protein turnover, and induction in the neuronal cells *in vitro*. *Neurotoxicology* 29: 232–243
- Cuervo AM, Dice JF (1996) A receptor for the selective uptake and degradation of proteins by lysosomes. *Science* 273: 501–503
- Cuervo AM, Dice JF (2000) Unique properties of lamp2a compared to other lamp2 isoforms. *J Cell Sci* 113: 4441–4450

- Dicthenberg JB, Zimmerman W, Sparks CA, Young A, Vidair C, Zheng Y, Carrington W, Fay FS, Doxsey SJ (1998) Pericentrin and γ -tubulin form a protein complex and are organized into a novel lattice at the centrosome. *J Cell Biol* 141: 163–174
- dos Santos FM, Gonçalves JCS, Caminha R, da Silveira GE, Neves CS, Gram KR, Ferreira CT, Jacqmin P, Noël F (2009) Pharmacokinetic/pharmacodynamic modeling of psychomotor impairment induced by oral clonazepam in healthy volunteers. *Ther Drug Monit* 31: 566–574
- Fortun J, Dunn Jr WA, Joy S, Li J, Notterpek L (2003) Emerging role for autophagy in the removal of aggregates in Schwann cells. *J Neurosci* 23: 10672–10680
- Franke WW, Schmid E, Osborn M, Weber K (1978) Different intermediate-sized filaments distinguished by immunofluorescence microscopy. *Proc Natl Acad Sci USA* 75: 5034–5038
- García-Mata R, Bebök Z, Sorscher EJ, Sztul ES (1999) Characterization and dynamics of aggregate formation by a cytosolic GFP-chimera. *J Cell Biol* 146: 1239–1254
- García-Mata R, Gao Y-S, Sztul ES (2002) Hassles with taking out the garbage: aggravating aggregates. *Traffic* 3: 388–396
- Gifondorwa DJ, Robinson MB, Hayes CD, Taylor AR, Prevetie DM, Oppenheim RW, Caress J, Milligan CE (2007) Exogenous delivery of heat shock protein 70 increases lifespan in a mouse model of amyotrophic lateral sclerosis. *J Neurosci* 27: 13173–13180
- Goetz MP, Toft D, Reid J, Ames M, Stensgard B, Safgren S, Adjei AA, Sloan J, Atherton P, Vasile V, Salazaar S, Adjei A, Croghan G, Erlichman C (2005) Phase I trial of 17-allylamino-17-demethoxygeldanamycin in patients with advanced cancer. *J Clin Oncol* 23: 1078–1087
- Guo F, Rocha K, Bali P, Pranpat M, Fiskus W, Boyapalle S, Kumaraswamy S, Balasis M, Greedy B, Armitage ESM, Lawrence N, Bhalla K (2005) Abrogation of heat shock protein 70 induction as a strategy to increase antileukemia activity of heat shock protein 90 inhibitor 17-allylamino-demethoxy geldanamycin. *Cancer Res* 65: 10536–10544
- Johnston JA, Ward CL, Kopito RR (1998) Aggregates: a cellular response to misfolded proteins. *J Cell Biol* 143: 1883–1898
- Kaushik S, Massey AC, Cuervo AM (2006) Lysosome membrane lipid microdomains: novel regulators of chaperone-mediated autophagy. *EMBO J* 25: 3921–3933
- Kawaguchi Y, Kovacs JJ, McLaurin A, Vance JM, Ito A, Yao T-P (2003) The deacetylase HDAC6 regulates aggregate formation and cell viability in response to misfolded protein stress. *Cell* 115: 727–738
- Kocher DK, Rawat N, Agrawal RP, Vyas A, Beniwal R, Kocher SK, Garg P (2004) Sodium valproate for painful diabetic neuropathy: a randomized double-blind placebo-controlled study. *QJM* 97: 33–38
- Kopito RR (2000) Aggregates, inclusion bodies and protein aggregation. *Trends Cell Biol* 10: 524–530
- Kumar SK, Rajkumar SV, Dispenzieri A, Lacy MQ, Hayman SR, Buadi FK, Zeldenrust SR, Dingli D, Russell SJ, Lust JA, Greipp PR, Kyle RA, Gertz MA (2008) Improved survival in multiple myeloma and the impact of novel therapies. *Blood* 111: 2516–2520
- Kyle RA, Rajkumar SV (2009) Treatment of multiple myeloma: a comprehensive review. *Clin Lymphoma Myeloma* 9: 278–288
- Mazumder A, Vesole DH, Jagannath S (2010) Vorinostat plus bortezomib for the treatment of relapsed/refractory multiple myeloma: a case series illustrating utility in clinical practice. *Clin Lymphoma Myeloma Leuk* 10: 149–151
- Meregalli C, Canta A, Carozzi VA, Chiorazzi A, Oggioni N, Gilardini A, Ceresa C, Avezza F, Crippa L, Marmiroli P, Cavaletti G (2010) Bortezomib-induced painful neuropathy in rats: a behavioral, neurophysiological and pathological study in rats. *Eur J Pain* 14: 343–350
- Mezey E, Dehejia A, Harta G, Papp MI, Polymeropoulos MH, Brownstein MJ (1998) Alpha synuclein in neurodegenerative disorders: murderer or accomplice? *Nat Med* 4: 755–757
- Mitsiades CS, Hideshima T, Chauhan D, McMillin DW, Klippel S, Laubach JP, Munshi NC, Anderson KC, Richardson PG (2009) Emerging treatments for multiple myeloma: beyond immunomodulatory drugs and bortezomib. *Semin Hematol* 46: 166–175
- Morimoto RI (1998) Regulation of the heat shock transcriptional response: cross talk between a family of heat shock factors, molecular chaperones, and negative regulators. *Genes Dev* 12: 3788–3796
- Munster P, Marchion D, Bicaku E, Lacevic M, Kim J, Centeno B, Daud A, Neuger A, Minton S, Sullivan D (2009) Clinical and biological effects of valproic acid as a histone deacetylase inhibitor on tumor and surrogate tissues: phase I/II trial of valproic acid and epirubicin/FEC. *Clin Cancer Res* 15: 2488–2496
- Nawrocki ST, Carew JS, Maclean KH, Courage JF, Huang P, Houghton JA, Cleveland JL, Giles FJ, McConkey DJ (2008) Myc regulates aggregate formation, the induction of Noxa, and apoptosis in response to the combination of bortezomib and SAHA. *Blood* 112: 2917–2926
- Ogawa Y, Tobinai K, Ogura M, Ando K, Tsuchiya T, Kobayashi Y, Watanabe T, Maruyama D, Morishima Y, Kagami Y, Taji H, Minami H, Itoh K, Nakata M, Hotta T (2008) Phase I and II pharmacokinetic and pharmacodynamic study of the proteasome inhibitor bortezomib in Japanese patients with relapsed or refractory multiple myeloma. *Cancer Sci* 99: 140–144
- Patel PI, Roa BB, Welcher AA, Schoener-Scott R, Trask BJ, Pentao L, Snipes GJ, Garcia CA, Francke U, Shooter EM, Lupski JR, Suter U (1992) The gene for the peripheral myelin protein PMP-22 is a candidate for Charcot-Marie-Tooth disease type 1A. *Nat Genet* 1: 159–165
- Richardson PG, Badros AZ, Jagannath S, Tarantolo S, Wolf JL, Albitar M, Berman D, Messina M, Anderson KC (2010) Tanespimycin with bortezomib: activity in relapsed/refractory patients with multiple myeloma. *Br J Haematol* 150: 428–437
- Richardson PG, Barlogie B, Berenson J, Singhal S, Jagannath S, Irwin D, Rajkumar SV, Srkalovic G, Alsina M, Alexanian R, Siegel D, Orlovski RZ, Kuter D, Limentani SA, Lee S, Hideshima T, Esseltine D-L, Kaufman M, Adams J, Schenkein DP, Anderson KC (2003) A phase 2 study of bortezomib in relapsed, refractory myeloma. *N Engl J Med* 348: 2609–2617
- Richardson PG, Briemberg H, Jagannath S, Wen PY, Barlogie B, Berenson J, Singhal S, Siegel DS, Irwin D, Schuster M, Srkalovic G, Alexanian R, Rajkumar SV, Limentani S, Alsina M, Orlovski RZ, Najarian K, Esseltine D, Anderson KC, Amato AA (2006) Frequency, characteristics, and reversibility of peripheral neuropathy during treatment of advanced multiple myeloma with bortezomib. *J Clin Oncol* 24: 3113–3120
- Richardson PG, Sonneveld P, Schuster MW, Stadtmauer EA, Facon T, Harousseau J-L, Ben-Yehuda D, Lonial S, Goldschmidt H, Reece D, Bladé J, Boccadoro M, Cavenagh JD, Boral AL, Esseltine D-L, Wen PY, Amato AA, Anderson KC, San Miguel J (2009a) Reversibility of symptomatic peripheral neuropathy with bortezomib in the phase III APEX trial in relapsed multiple myeloma: impact of a dose-modification guideline. *Br J Haematol* 144: 895–903
- Richardson PG, Xie W, Mitsiades C, Chanan-Khan AA, Lonial S, Hassoun H, Avigan DE, Oaklander AL, Kuter DJ, Wen PY, Kesari S, Briemberg HR, Schlossman RL, Munshi NC, Heffner LT, Doss D, Esseltine D-L, Weller E, Anderson KC, Amato AA (2009b) Single-agent bortezomib in previously untreated multiple myeloma: efficacy, characterization of peripheral neuropathy, and molecular correlations with response and neuropathy. *J Clin Oncol* 27: 3518–3525
- Roodveldt C, Bertoncini CW, Andersson A, van der Goot AT, Hsu S-T, Fernández-Montesinos R, de Jong J, van Ham TJ, Nollen EA, Pozo D, Christodoulou J, Dobson CM (2009) Chaperone proteostasis in Parkinson's disease: stabilization of the Hsp70/ α -synuclein complex by Hip. *EMBO J* 28: 3758–3770
- San Miguel JF, Schlag R, Khuageva NK, Dimopoulos MA, Shpilberg O, Kropf M, Spicka I, Petrucci MT, Palumbo A, Samoilova OS, Dmoszynska A, Abdulkadyrov KM, Schots R, Jiang B, Mateos M-V, Anderson KC, Esseltine DL, Liu K, Cakana A, van de Velde H, Richardson PG, for the VISTA Trial Investigators (2008) Bortezomib plus melphalan and prednisone for initial treatment of multiple myeloma. *N Engl J Med* 359: 906–917
- Scuteri A, Nicolini G, Miloso M, Bossi M, Cavaletti G, Windebank AJ, Tredici G (2006) Paclitaxel toxicity in post-mitotic dorsal root ganglion (DRG) cells. *Anticancer Res* 26: 1065–1070
- Shen S, Zhang P, Lovchik MA, Li Y, Tang L, Chen Z, Zeng R, Ma D, Yuan J, Yu Q (2009) Cyclodepsipeptide toxin promotes the degradation of Hsp90 client proteins through chaperone-mediated autophagy. *J Cell Biol* 185: 629–639
- Wacker JL, Huang S-Y, Steele AD, Aron R, Lotz GP, Nguyen QV, Giorgini F, Roberson ED, Lindquist S, Maslah E, Muchowski PJ (2009) Loss of Hsp70 exacerbates pathogenesis but not levels of fibrillar aggregates in a mouse model of Huntington's disease. *J Neurosci* 29: 9104–9114
- Watanabe T, Kato H, Kobayashi Y, Yamasaki S, Morita-Hoshi Y, Yokoyama H, Morishima Y, Ricker JL, Otsuki T, Miyagi-Maesima A, Matsuno Y, Tobinai K (2010) Potential efficacy of the oral histone deacetylase inhibitor vorinostat in a phase I trial in follicular and mantle cell lymphoma. *Cancer Sci* 101: 196–200
- Zou J, Guo Y, Guettouche T, Smith DF, Voellmy R (1998) Repression of heat shock transcription factor HSF1 activation by HSP90 (HSP90 complex) that forms a stress-sensitive complex with HSF1. *Cell* 94: 471–480

Bortezomib potentially inhibits cellular growth of vascular endothelial cells through suppression of G2/M transition

Daisuke Tamura,^{1,2} Tokuzo Arao,¹ Kaoru Tanaka,¹ Hiroyasu Kaneda,¹ Kazuko Matsumoto,¹ Kanae Kudo,¹ Keiichi Aomatsu,¹ Yoshihiko Fujita,¹ Takashi Watanabe,³ Nagahiro Saijo,³ Yoshikazu Kotani,² Yoshihiro Nishimura² and Kazuto Nishio^{1,4}

¹Department of Genome Biology, Kinki University School of Medicine, Osaka; ²Division of Respiratory Medicine, Department of Internal Medicine, Kobe University Graduate School of Medicine, Kobe; ³Division of Medical Oncology, National Cancer Center Hospital, Japan

(Received January 13, 2010/Revised February 12, 2010/Accepted February 21, 2010/Accepted manuscript online February 27, 2010/Article first published online March 29, 2010)

Bortezomib, a selective 26S proteasome inhibitor, has shown clinical benefits against refractory multiple myeloma. The indirect anti-angiogenic activity of bortezomib has been widely recognized; however, the growth-inhibitory mechanism of bortezomib on vascular endothelial cells remains unclear, especially on the cell cycle. Here, we showed that bortezomib (2 nM of the IC₅₀ value) potently inhibited the cellular growth of human umbilical vascular endothelial cells (HUVECs) via a vascular endothelial growth factor receptor (VEGFR)-independent mechanism resulting in the induction of apoptosis. Bortezomib significantly increased the vascular permeability of HUVECs, whereas a VEGFR-2 tyrosine kinase inhibitor decreased it. Interestingly, a cell cycle analysis using flow cytometry, the immunostaining of phospho-histone H3, and Giemsa staining revealed that bortezomib suppressed the G2/M transition of HUVECs, whereas the mitotic inhibitor paclitaxel induced M-phase accumulation. A further analysis of cell cycle-related proteins revealed that bortezomib increased the expression levels of cyclin B1, the cdc2/cyclin B complex, and the phosphorylation of all T14, Y15, and T161 residues on cdc2. Bortezomib also increased the ubiquitination of cyclin B1 and wee1, but inhibited the kinase activity of the cdc2/cyclin B complex. These protein modifications support the concept that bortezomib suppresses the G2/M transition, rather than causing M-phase arrest. In conclusion, we demonstrated that bortezomib potently inhibits cell growth by suppressing the G2/M transition, modifying G2/M-phase-related cycle regulators, and increasing the vascular permeability of vascular endothelial cells. Our findings reveal a cell cycle-related mode of action and strongly suggest that bortezomib exerts an additional unique vascular disrupting effect as a vascular targeting drug. (*Cancer Sci* 2010; 101: 1403–1408)

The proteasome is an essential enzyme complex for nonlysosomal and ATP-dependent proteolytic pathways. The ubiquitin–proteasome pathway plays an important role in the intracellular degradation of damaged, oxidized, or misfolded proteins^(1–4) as well as in the cell cycle progression. Such damaged, oxidized, or misfolded proteins have been identified as substrates for the ubiquitin/proteasome system.^(1,5–7) In addition, this system has been implicated in the regulation of cell proliferation, differentiation, survival, apoptosis, and angiogenesis.^(8,9) Because of these unique effects of the proteasome/ubiquitin system on cellular regulation, the proteasome is a novel and promising target for cancer therapy.^(10–12)

Bortezomib (Velcade, PS-341), a selective 26S proteasome inhibitor, demonstrates potent antitumor activity against several human cancers and has been clinically used mainly in patients with refractory multiple myeloma.^(13–15) The main mechanism of action of this drug was initially thought to be

the inhibition of nuclear factor- κ B (NF- κ B), which acts as a transcription factor for anti-apoptotic proteins, such as Bcl-2, c-IAP2, and survivin. Accumulating data indicates that bortezomib disrupts the cell cycle by modifying cyclins and inhibits the up-regulation of interleukin-6 (IL-6), which plays an important role in the proliferation of myeloma cells, by inhibiting NF- κ B and stabilizing p53, p21, and p27, resulting in its anticancer activity.^(1,16–18)

Bortezomib exerts an anti-angiogenic effect by decreasing the secretion of vascular endothelial growth factor (VEGF) from myeloma cells.^(19,20) This anti-angiogenic effect of bortezomib is considered an indirect effect on vascular endothelial cells resulting from ligand depletion. Meanwhile, direct negative proliferative effects of bortezomib on vascular endothelial cells have emerged which play an important role in its anti-angiogenic activity. Roccaro *et al.*⁽⁹⁾ reported that bortezomib induces inhibition of angiogenesis in functional assays of angiogenesis, including chemotaxis, adhesion to fibronectin, capillary formation on Matrigel, and chick embryo chorioallantoic membrane assay using multiple myeloma patient-derived endothelial cells and human umbilical vein endothelial cells (HUVECs). Podar *et al.*⁽²¹⁾ reported that Caveolin-1 is a molecular target of bortezomib in multiple myeloma cells and HUVECs and this is required for VEGF-triggered multiple myeloma. However the underlying mechanism responsible for the direct negative proliferative effect of bortezomib on vascular endothelial cells remains unclear, especially with regard to its effect on the cell cycle.

To gain insight into the direct anti-angiogenic effects of bortezomib on HUVECs, we examined cellular proliferation, tube formation, VEGF receptor-2 (VEGFR-2) signaling, the apoptotic pathway, vascular permeability, cell cycle analysis, and effects of drugs on cell cycle-related proteins.

Materials and Methods

Anticancer agents. Bortezomib was provided by Millennium Pharmaceuticals (Cambridge, MA, USA). The VEGFR-2 tyrosine kinase inhibitor (VEGFR-2-TKI) Ki8751 (IC₅₀ value for VEGFR-2 kinase inhibition = 0.90 nM) was purchased from Sigma (St. Louis, MO, USA). Paclitaxel was purchased from Wako Pure Chemical Industries (Osaka, Japan). Each chemical agent was dissolved in dimethylsulfoxide for use in the *in vitro* experiments.

⁴To whom correspondence should be addressed.
E-mail: knishio@med.kindai.ac.jp

Cell cultures. HUVECs were maintained in Humedia-EG2 (Kurabo, Tokyo, Japan) with 2% fetal bovine serum and 0.1% gentamicin-amphotericinB with the addition of 10 ng/mL of epidermal growth factor, 5 ng/mL of fibroblast growth factor, and 2 ng/mL of VEGF (R&D Systems, Minneapolis, MN, USA). All the cell lines were incubated at 37°C with humidified 5% CO₂.

In vitro growth inhibition assay. Growth inhibition was evaluated using the MTT assay, as described previously.⁽²²⁾ The experiment was performed in triplicate.

Western blotting. The antibodies used for western blotting were anti-phospho-VEGFR-2 (Tyr1175), anti-VEGFR-2, anti-MAPK, anti-phospho-MAPK, anti-β-actin, anti-cleaved or non-cleaved-caspase3, anti-cleaved or non-cleaved-poly ADP-ribose polymerase (PARP), anti-cyclin B1, anti-phospho-cdc2, anti-cdc2, anti-phospho-wee1, anti-wee1, anti-phospho-cdc25C, anti-cdc25C, anti-phospho-chk1 and -2, and anti-chk1 and -2 (Cell Signaling, Beverly, MA, USA). HUVECs were cultured overnight in serum-starved medium and then exposed to the indicated concentrations of bortezomib or Ki8751 for 3 h before the addition of 10 ng/mL of VEGF for 5 min. The western blot analysis was performed as described previously.⁽²³⁾ The experiment was performed in duplicate.

Immunoprecipitation. Total cell lysates were immunoprecipitated with anti-wee1, cdc2 antibodies (Cell Signaling), or anti-cyclin B1 antibody (Santa Cruz Biotechnology, Santa Cruz, CA, USA) overnight at 4°C. The protein complex was incubated with protein G-agarose (Invitrogen, San Diego, CA, USA) for 1 h at 4°C and washed three times with lysis buffer. After sequential centrifugation and washing, the pellets were resuspended in 1.5 × sample loading buffer and subjected to immunoblot analyses.

Cell cycle analysis. Cells were treated with the indicated concentrations of bortezomib for 24 h. The cells were then harvested, washed with PBS, fixed with 70% ethanol at -20°C overnight, washed again with PBS, and then stained with 5 μg/mL of propidium iodide containing 0.1% Triton X-100, 0.1 mM EDTA, and RNase I (BD Bioscience, San Jose, CA, USA). The stained cells were then analyzed for DNA content using a FACS Calibur flow cytometer (BD Biosciences) and the cell cycle distributions were calculated using ModFit LT software. The experiment was performed in triplicate.

Giemsa staining. Morphological changes in mitotic cells were evaluated using Giemsa staining. HUVECs treated with bortezomib (1 μM) or paclitaxel (1 μM) for 24 h were fixed with 10% neutral-buffered formaldehyde before staining and were stained for 30 min, then washed with tap water for 5 min. The morphological changes were evaluated using a light microscope (×40).

Immunofluorescence staining of phospho-histone H3. HUVECs were treated with 1 μM of bortezomib or paclitaxel for 24 h and were then fixed and permeabilized with 4% formaldehyde/PBS for 15 min. The cells were blocked with 5% normal goat serum in PBS for 60 min. After washing, anti-phospho-histone H3 antibody (Cell Signaling) was diluted 1:200 in PBS/Triton and incubated for 1 h at room temperature, followed by detection using Alexa Fluor 594 goat antirabbit IgG antibody (Invitrogen) for 1 h. After washing, the cells were counterstained with 1 μg/mL of 4',6-diamidino-2-phenylindole (DAPI) in PBS for 5 min. Images were obtained using fluorescence microscopy (IX71; Olympus, Tokyo, Japan). The mitotic index was calculated by dividing the number of p-Histone H3-positive cells by the total number of treated cells (DAPI-positive cells). At least 100 cells were scored per low-power field, and the cells were counted over three fields. The experiment was performed in triplicate.

cdc2/cyclinB1 kinase assay. The cdc2/cyclinB1 kinase activity in the cells was quantified using a Cyclex Cdc2-CylinB Kinase Assay Kit (Cyclex, Nagano, Japan) according to the

manufacturer's instructions. The experiment was performed in triplicate.

In vitro permeability assay. Transwell permeability assays were performed using monolayers of HUVECs and an *in vitro* vascular permeability assay kit (Chemicon, Temecula, CA, USA). Briefly, HUVECs seeded onto collagen-coated inserts were pretreated with or without bortezomib (1, 0.1 μM) or VEGFR-2-TKI (1 μM) for 6 h, and VEGF (20 ng/mL) was added, except in the control sample, 4 h thereafter. Two hours after the addition of VEGF, fluorescein isothiocyanate dextran (FITC dextran) was added on the top of the cells and the extent of FITC dextran permeation was determined by measuring the fluorescence of the plate well solution, according to the supplier's instructions. The experiment was performed in triplicate.

Results

Bortezomib potentially inhibited the cellular growth of HUVECs independent of VEGF signaling. To evaluate the growth inhibitory activity of bortezomib *in vitro*, we performed MTT assays on HUVECs under the 20 ng/mL of VEGF or without it. Bortezomib exhibited a potent growth inhibitory activity on HUVECs with an IC₅₀ of 2 nM; however, VEGF stimulation did not influence the growth inhibitory activity of bortezomib (Fig. 1a).

To address the question whether the growth inhibitory activity of bortezomib involves VEGFR-2 signaling, we compared the inhibitory effects of bortezomib with that of a VEGFR-2-TKI, Ki8751, on the phosphorylation levels of VEGFR and MAPK. Bortezomib did not inhibit the phosphorylation level of VEGFR-2, whereas Ki8751 (0.01–1 μM) completely inhibited VEGFR-2 phosphorylation (Fig. 1b). Similar results were observed for MAPK phosphorylation. These results indicate that the growth inhibitory activity of bortezomib is induced via a VEGFR-2 signaling-independent mechanism.

Bortezomib increases vascular permeability in vitro. Generally, the characteristics of vascular disrupting agents include a potent anti-proliferative effect. Microtubule-binding drugs (MBD) are widely used in cancer chemotherapy and also have clinically relevant vascular-disrupting properties. The disruption of adherens junctions contributes to the rounding of endothelial cells, leading to a direct increase in vasculature permeability.⁽²⁴⁾ Therefore, we examined the effect of bortezomib on vasculature permeability to gain an insight into its vascular-disrupting properties. As expected, Ki8751 significantly decreased vasculature permeability during VEGF stimulation, in contrast to the situation in untreated controls. On the other hand, bortezomib significantly increased the vasculature permeability of vasculature endothelial cells in a dose-dependent manner (Fig. 1c). This result supports the hypothesis that bortezomib has vascular-disrupting properties in HUVECs in addition to its potent growth inhibitory effect.

Bortezomib induces apoptosis of HUVECs. We speculated that the potent growth inhibitory activity of bortezomib was based on the induction of apoptosis; thus, we evaluated the expression levels of cleaved caspase 3, cleaved PARP, and ubiquitinated protein from whole cell lysates. The expression levels of cleaved caspase 3 and PARP showed that bortezomib induced the activation of caspase 3 at a dose of 0.1 μM and subsequent PARP cleavage in HUVECs in a dose- and time-dependent manner (Fig. 2). The accumulation of ubiquitinated proteins, which represents a direct effect of bortezomib, was observed at 0.01 μM in a time-dependent manner. These findings indicate that bortezomib is capable of inducing the apoptosis of HUVECs at a relatively low concentration.

Bortezomib inhibits G2/M transition. An analysis of the cell cycle distribution of HUVECs revealed that bortezomib significantly increased the population of cells in the G2/M phase

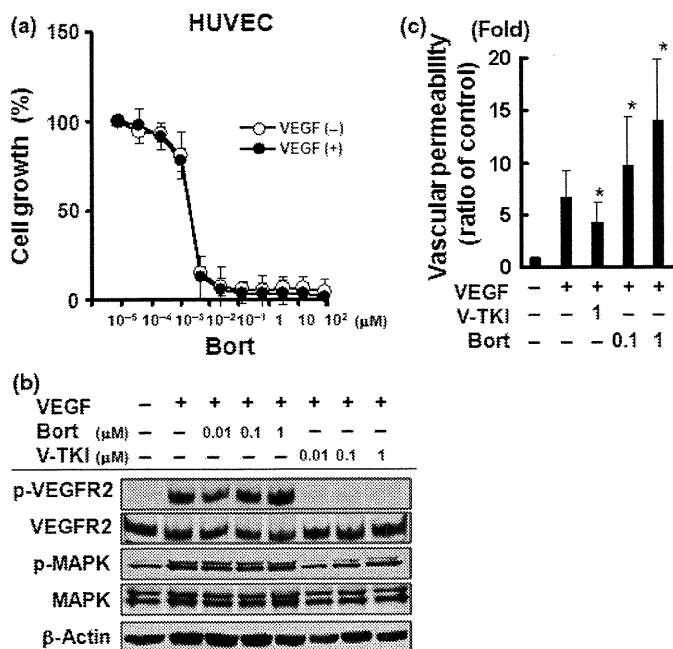


Fig. 1. Bortezomib potently inhibited the cellular growth and increased the vascular permeability of HUVECs. (a) *In vitro* growth-inhibitory effect of bortezomib on HUVECs using an MTT assay with 10 ng/mL vascular endothelial growth factor (VEGF) or without it. The data shown represents the average \pm SD of three independent experiments. (b) Effects of bortezomib on VEGF signaling in HUVECs. Western blot analysis was performed for the expression and phosphorylation levels of VEGF receptor-2 (VEGFR-2) and MAPK. HUVECs were cultured under serum-starved conditions and exposed to bortezomib or Ki8751 at the indicated concentrations for 3 h. After 10 ng/mL VEGF stimulation for 5 min, the cells were analyzed. (c) Effect of bortezomib on vascular permeability *in vitro*. HUVECs were seeded onto collagen-coated inserts and were pretreated with or without bortezomib (0.1 and 1 μ M) or VEGFR-2 tyrosine kinase inhibitor (VEGFR-2-TKI) (1 μ M) for 6 h. After 20 ng/mL of VEGF stimulation for 2 h, fluorescein isothiocyanate dextran (FITC dextran) was added on the top of the inserts and the extent of FITC dextran permeation was determined by measuring the fluorescence of the plate well solution. The relative vascular permeability was calculated using the ratio to the permeability in the control cells (untreated). The data shown represents the average \pm SD of three independent experiments. * P < 0.05. Bort, bortezomib; V-TKI, VEGFR-2-TKI.

(Fig. 3a). This effect was observed when the cells were exposed to 0.01 μ M of bortezomib. Generally, morphological changes, including the disappearance of the nuclear membrane, chromosomal condensation, and cytoplasmic round formation, are observed in mitotic cells. Therefore, we evaluated whether bort-

ezomib induced morphological changes in HUVECs specific to mitotic cells. Paclitaxel, a well-known tubulin binder and mitotic inhibitor, was used as a control. Paclitaxel clearly induced these morphological changes specific to mitotic cells; however, bortezomib did not induce these changes with Giemsa staining (Fig. 3b). Further analysis using phospho-histone H3 immunostaining, an M-phase-specific marker, demonstrated that bortezomib significantly decreased the number of mitotic cells while paclitaxel markedly increased it (Fig. 3c,d). Together, these results indicated that both bortezomib and paclitaxel induced cell cycle arrest at the G2/M phase; however, bortezomib did not increase the number of mitotic cells unlike paclitaxel. These results suggest that bortezomib inhibits the G2/M transition in HUVECs.

Bortezomib decreases cdc2/cyclin B kinase activity. Cell cycle progression at the G2/M transition is regulated by cdc2/cyclin B complex activity, and the activation of this complex is controlled as a consecutive process as follows: (i) the levels of cyclin B protein are increased during late S and G2 phases; (ii) cyclin B binds to unphosphorylated cdc2 and forms an inactive cdc2/cyclin B complex; (iii) cdc2 is phosphorylated at its T14, Y15, and T161 residues during the G2 phase; and (iv) the dephosphorylation of T14 and Y15 on cdc2 by phosphatase cdc25 activates the cdc2/cyclin B complex and introduces the cells to mitosis.

Bortezomib increased the expression of cyclin B1 in a dose- and time-dependent manner, and an immunoprecipitation analysis showed that bortezomib also increased the production of cdc2/cyclin B complexes (Fig. 4a). Bortezomib markedly increased the phosphorylation status of the T14, Y15, and T161 residues on cdc2 in a dose- and time-dependent manner, suggesting that bortezomib promoted the presence of the inactive form of the cdc2/cyclin B complex (Fig. 4b). These results showed that bortezomib inhibits the G2/M transition. In addition, we examined the effects on a competing kinase, wee1, and the phosphatase cdc25C. Increased expression and phosphorylation levels of wee1 were observed after bortezomib treatment, whereas no remarkable changes in cdc25C expression or phosphorylation were observed (Fig. 4b). Regarding the effects of bortezomib on the proteasome-ubiquitin pathway, we found that the ubiquitination of wee1 and cyclin B protein was increased by bortezomib in a dose-dependent manner, suggesting that the increase in the ubiquitination of wee1 and cyclin B may be at least partially involved in the suppression of the G2/M transition and the mode of action of this drug (Fig. 5a). Finally, a kinase assay of the cdc2/cyclin B complex showed that bortezomib (0.01 μ M) significantly inhibited the kinase activity of the complex, indicating that the inhibition of kinase activity might suppress the G2/M transition (Fig. 5b).

Together, these results revealed that bortezomib increases the expression levels of cyclin B1, the formation of the cdc2/cyclin

Fig. 2. Bortezomib induces apoptosis of HUVECs. Western blot analysis was performed for the cleaved form and the expression levels of caspase 3, poly ADP-ribose polymerase (PARP), and whole ubiquitinated-protein. HUVECs were treated with bortezomib at the indicated concentrations for 24 h and analyzed (left panel), or they were treated with bortezomib at 0.1 μ M for the indicated hours (right panel). Protein size markers are shown at 100 and 220 kDa.



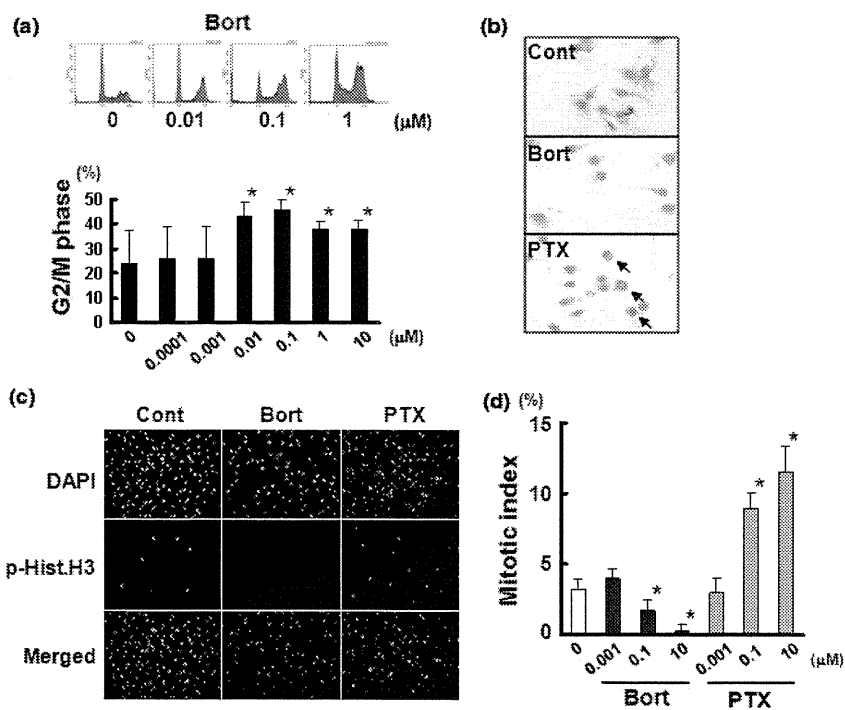


Fig. 3. Bortezomib suppresses the G2/M transition. (a) DNA histogram of HUVECs treated with bortezomib. HUVECs were treated with bortezomib at the indicated concentrations. The upper panel represents the result of a flow cytometry analysis, and the lower panel shows the population at the G2/M phase. $*P < 0.05$. (b) Giemsa staining of HUVECs treated with bortezomib or paclitaxel at 1 μM . The arrows indicate cells with mitotic changes (disappearance of the nuclear membrane, chromosomal condensation, and cytoplasmic round formation). (c) Immunostaining for phospho-histone H3 (p-Hist.H3) and 4',6-diamidino-2-phenylindole (DAPI) observed with fluorescence microscopy. p-Hist.H3 was used as an M-phase-specific molecular marker. Note that both bortezomib and paclitaxel induced cell cycle arrest at the G2/M phase, but unlike paclitaxel, bortezomib did not increase the number of cells in the M phase. (d) Mitotic index after treatment with bortezomib or paclitaxel at the indicated concentrations in HUVECs. The mitotic index was calculated using the number of p-Hist.H3-positive cells per the total number of cells (DAPI-positive cells). The columns indicate the average \pm SD of three independent experiments. $*P < 0.05$. Bort, bortezomib; Cont, untreated control; PTX, paclitaxel.

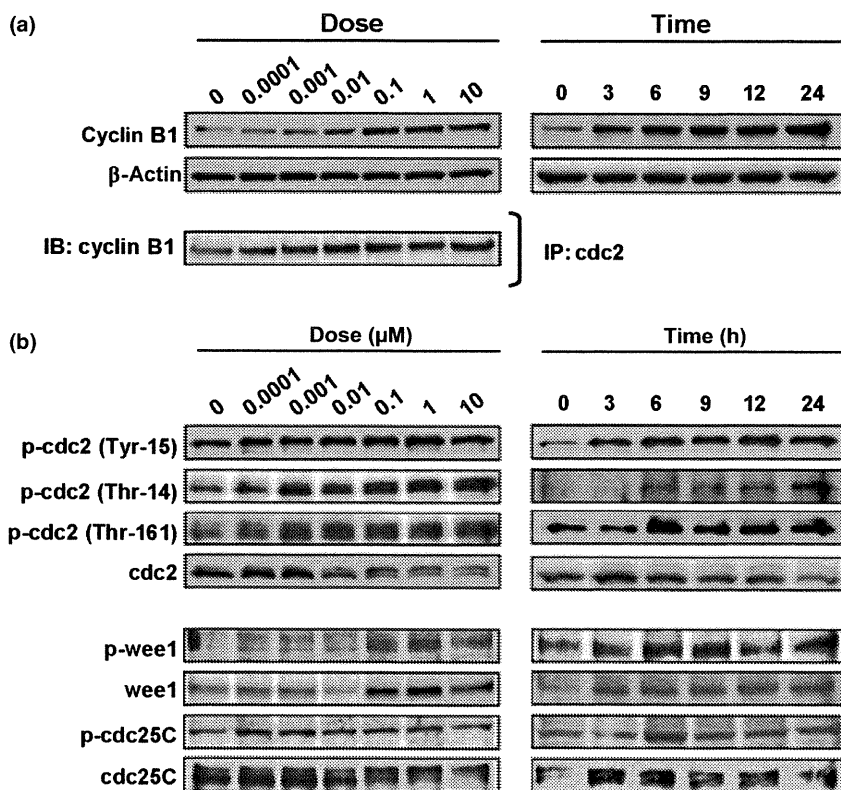


Fig. 4. Bortezomib increases the expression levels of cyclin B1, the production of the cdc2/cyclin B complex, and the phosphorylation of the T14, Y15, and T161 residues on cdc2 in HUVECs. (a) Western blots of the cyclin B1 expression levels in whole protein (upper panel) and samples immunoprecipitated with a cdc2 antibody (lower panel). (b) Western blots for G2/M-phase-related cell cycle regulators. HUVECs were treated with bortezomib at the indicated concentrations for 24 h and for the indicated hours at 0.1 μM . IB, immunoblots; IP, immunoprecipitation.

B complex, the phosphorylation of T14, Y15 and T161 residues on cdc2, and the ubiquitination of cyclin B1 and wee1. Bortezomib also significantly inhibited the kinase activity of cdc2/cyclin B. These modifications of G2/M-phase-related cell cycle regulators suggest that bortezomib suppresses the G2/M transition (Fig. 5c). We concluded that bortezomib potently inhibits cell growth of vascular endothelial cells by suppressing the

G2/M transition through modifying G2/M-phase-related cycle regulators.

Discussion

Inhibition of the 26S proteasome results in the accumulation of cyclins A, B, D, E, p21, and p27, thereby disrupting the cell

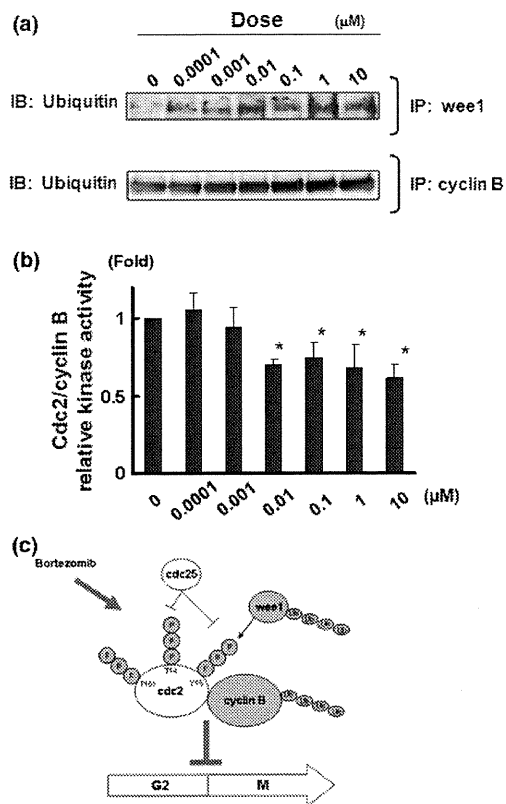


Fig. 5. Bortezomib increases the ubiquitination of cyclin B1 and wee1 and inhibits the kinase activity of cdc2/cyclin B. (a) Western blots for the ubiquitination levels in the samples immunoprecipitated with wee1 antibody (lower panel) or cyclin B1 antibody (lower panel). (b) Kinase activity of cdc2/cyclin B in HUVECs treated with bortezomib at the indicated concentrations. Whole cell lysates were used for the analysis. The relative kinase activity was calculated using the ratio to the activity level in the control (untreated). The data shown represents the average \pm SD of three independent experiments. * $P < 0.05$. (c) Schematic diagram of the effects of bortezomib on G2/M-phase cell cycle progression in vascular endothelial cells. Bortezomib increases the expression levels of cyclin B1, the production of the cdc2/cyclin B complex, and the phosphorylation of the T14, Y15, and T161 residues on cdc2. Bortezomib also increases the ubiquitination of cyclin B1 and wee1. Changes in the expression or phosphorylation levels of cdc2 were not detected. These modifications of G2/M-phase-related cell cycle regulators suggest that bortezomib suppresses the G2/M transition.

cycle and promoting cell death via multiple pathways.⁽²⁵⁾ In cancer cells, bortezomib leads to an increase in the accumulation and activation of G2/M-phase-related cell cycle regulators cyclin A and cyclin B1, and also leads to cell cycle blockade at the G2/M phase.⁽¹⁾ However, whether bortezomib inhibits G2/M transition or induces M-phase arrest has been uncertain. In addition, no data on the effects of bortezomib on the cell cycle arrest at the G2 phase in vascular endothelial cells has been available.

References

- Ling YH, Liebes L, Jiang JD *et al*. Mechanisms of proteasome inhibitor PS-341-induced G(2)-M-phase arrest and apoptosis in human non-small cell lung cancer cell lines. *Clin Cancer Res* 2003; **9**: 1145–54.
- Hochstrasser M. Ubiquitin, proteasomes, and the regulation of intracellular protein degradation. *Curr Opin Cell Biol* 1995; **7**: 215–23.
- Jentsch S, Schlenker S. Selective protein degradation: a journey's end within the proteasome. *Cell* 1995; **82**: 881–4.

Our data showed that bortezomib caused cell cycle arrest at the G2 phase, not at the M phase, using Giemsa staining and immunofluorescence staining of the phospho-histone H3 in HUVECs (Fig. 3). Because bortezomib inhibits the G2/M transition, we focused on changes in G2/M-phase-related cell cycle regulators, such as cyclin B and cdc2. We found that bortezomib increased the expression levels of cyclin B, ubiquitinated cyclin B, and the cyclin B/cdc2 complex in dose- and time-dependent manners (Figs 4 and 5a). Further analysis revealed that the phosphorylation statuses of the T14, Y15, and T161 residues on cdc2 were markedly increased, indicating the presence of the inactive form of cdc2 that occurs during G2 arrest; the kinase activity of the cyclin B/cdc2 complex was also inhibited by this treatment (Figs 4b,5b). These data indicate that bortezomib inhibits the G2/M transition, rather than causing M-phase arrest. Since few anticancer drugs are known to suppress the G2/M transition, our results provide an insight to the unique mode of action of bortezomib. The expression, ubiquitination, and phosphorylation of wee1 were markedly increased after bortezomib treatment. Wee1 degrades via the proteasome-ubiquitin pathway, similar to cyclin B, and activated wee1 inhibits cdc2 kinase activity. Therefore, these results raise the possibility that wee1 is involved in the mode of action of bortezomib.

Vascular targeting agents (VTAs) including VEGFR-TKIs target the development of new vessels and have a preventative action, require chronic administration, and are likely to be of particular benefit in early stage or asymptomatic metastatic disease. Meanwhile, vascular disrupting agents (VDAs) target established tumor blood vessels,⁽²⁶⁾ causing a rapid collapse in tumor blood flow leading to a prolonged period of vascular shut-down and culminating in the extensive necrosis of tumor cells.⁽²⁷⁾ VDAs are therefore given acutely, show immediate effects, and may have particular efficacy against advanced disease. Thus, VDAs are considered to be different from VTAs in some key aspects including the type or extent of disease which has sensitivity to the agents and the treatment scheduling.⁽²⁶⁾

Generally, the characteristics of VDAs include a potent anti-proliferative effect, the induction of G2/M-phase arrest, and an increase in vascular permeability.⁽²⁸⁾ Our results indicate that bortezomib exerts similar effects on vascular endothelial cells. Thus, we speculate that bortezomib could be categorized as a VDA and that the vascular disrupting effect of bortezomib might be at least partly responsible for its antitumor activity.

In conclusion, we demonstrated that bortezomib potently inhibits cellular growth by suppressing the G2/M transition in vascular endothelial cells. Our findings strongly suggest that bortezomib has a unique additional vascular disrupting effect.

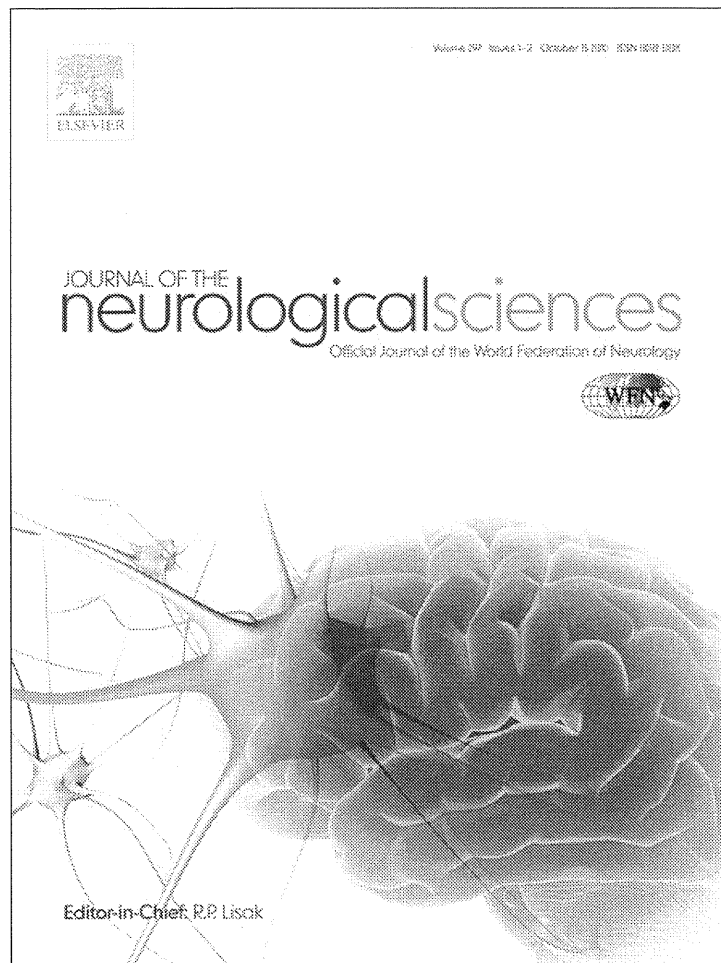
Acknowledgments

We thank Mr Shinji Kurashimo, Mr Yoshihiro Mine, and Ms Tomoko Kitayama for their technical assistance. This work was supported in part by the Third-Term Comprehensive 10-Year Strategy for Cancer Control, the Program for the Promotion of Fundamental Studies in Health Sciences of the National Institute of Biomedical Innovation (NiBio), funds for Health and Labor Scientific Research Grants, and a Grant-in-Aid for Scientific Research (A).

- Hershko A, Ciechanover A. The ubiquitin system. *Annu Rev Biochem* 1998; **67**: 425–79.
- Desai SD, Liu LF, Vazquez-Abad D, D'Arpa P. Ubiquitin-dependent destruction of topoisomerase I is stimulated by the antitumor drug camptothecin. *J Biol Chem* 1997; **272**: 24159–64.
- Ciechanover A, DiGiuseppe JA, Bercovich B *et al*. Degradation of nuclear oncoproteins by the ubiquitin system in vitro. *Proc Natl Acad Sci U S A* 1991; **88**: 139–43.

- 7 Treier M, Staszewski LM, Bohmann D. Ubiquitin-dependent c-Jun degradation in vivo is mediated by the delta domain. *Cell* 1994; **78**: 787–98.
- 8 Grimm LM, Goldberg AL, Poirier GG, Schwartz LM, Osborne BA. Proteasomes play an essential role in thymocyte apoptosis. *EMBO J* 1996; **15**: 3835–44.
- 9 Roccaro AM, Hideshima T, Raje N *et al*. Bortezomib mediates antiangiogenesis in multiple myeloma via direct and indirect effects on endothelial cells. *Cancer Res* 2006; **66**: 184–91.
- 10 Rajkumar SV, Richardson PG, Hideshima T, Anderson KC. Proteasome inhibition as a novel therapeutic target in human cancer. *J Clin Oncol* 2005; **23**: 630–9.
- 11 Mani A, Gelmann EP. The ubiquitin-proteasome pathway and its role in cancer. *J Clin Oncol* 2005; **23**: 4776–89.
- 12 Genini D, Carbone GM, Catapano CV Multiple Interactions between Peroxisome Proliferators-Activated Receptors and the Ubiquitin-Proteasome System and Implications for Cancer Pathogenesis. *PPAR Res* 2008; **2008**: 195065.
- 13 APEX (Assessment of Proteasome inhibition for Extending remissions) trial: phase III randomized, multicenter, placebo-controlled trial to evaluate the efficacy and safety of bortezomib versus dexamethasone in patients with recurrent or treatment-resistant multiple myeloma. *Clin Adv Hematol Oncol* 2003; **1**: 190.
- 14 Jung L, Holle L, Dalton WS. Discovery, Development, and clinical applications of bortezomib. *Oncology (Williston Park)* 2004; **18**: 4–13.
- 15 Richardson PG, Sonneveld P, Schuster MW *et al*. Bortezomib or high-dose dexamethasone for relapsed multiple myeloma. *N Engl J Med* 2005; **352**: 2487–98.
- 16 Pham LV, Tamayo AT, Yoshimura LC, Lo P, Ford RJ. Inhibition of constitutive NF-kappa B activation in mantle cell lymphoma B cells leads to induction of cell cycle arrest and apoptosis. *J Immunol* 2003; **171**: 88–95.
- 17 Hideshima T, Richardson P, Chauhan D *et al*. The proteasome inhibitor PS-341 inhibits growth, induces apoptosis, and overcomes drug resistance in human multiple myeloma cells. *Cancer Res* 2001; **61**: 3071–6.
- 18 Strauss SJ, Higginbottom K, Juliger S *et al*. The proteasome inhibitor bortezomib acts independently of p53 and induces cell death via apoptosis and mitotic catastrophe in B-cell lymphoma cell lines. *Cancer Res* 2007; **67**: 2783–90.
- 19 Hayashi T, Hideshima T, Anderson KC. Novel therapies for multiple myeloma. *Br J Haematol* 2003; **120**: 10–7.
- 20 Hideshima T, Chauhan D, Podar K, Schlossman RL, Richardson P, Anderson KC. Novel therapies targeting the myeloma cell and its bone marrow microenvironment. *Semin Oncol* 2001; **28**: 607–12.
- 21 Podar K, Shringarpure R, Tai YT *et al*. Caveolin-1 is required for vascular endothelial growth factor-triggered multiple myeloma cell migration and is targeted by bortezomib. *Cancer Res* 2004; **64**: 7500–6.
- 22 Takeda M, Arai T, Yokote H *et al*. AZD2171 shows potent antitumor activity against gastric cancer over-expressing fibroblast growth factor receptor 2/keratinocyte growth factor receptor. *Clin Cancer Res* 2007; **13**: 3051–7.
- 23 Matsumoto K, Arai T, Tanaka K *et al*. mTOR signal and hypoxia-inducible factor-1 alpha regulate CD133 expression in cancer cells. *Cancer Res* 2009; **69**: 7160–4.
- 24 Schwartz EL. Antivascular actions of microtubule-binding drugs. *Clin Cancer Res* 2009; **15**: 2594–601.
- 25 Leonard JP, Furman RR, Coleman M. Proteasome inhibition with bortezomib: a new therapeutic strategy for non-Hodgkin's lymphoma. *Int J Cancer* 2006; **119**: 971–9.
- 26 Lippert JW III. Vascular disrupting agents. *Bioorg Med Chem* 2007; **15**: 605–15.
- 27 Tozer GM, Kanthou C, Baguley BC. Disrupting tumour blood vessels. *Nat Rev Cancer* 2005; **5**: 423–35.
- 28 Siemann DW, Bibby MC, Dark GG *et al*. Differentiation and definition of vascular-targeted therapies. *Clin Cancer Res* 2005; **11**: 416–20.

Provided for non-commercial research and education use.
Not for reproduction, distribution or commercial use.



This article appeared in a journal published by Elsevier. The attached copy is furnished to the author for internal non-commercial research and education use, including for instruction at the authors institution and sharing with colleagues.

Other uses, including reproduction and distribution, or selling or licensing copies, or posting to personal, institutional or third party websites are prohibited.

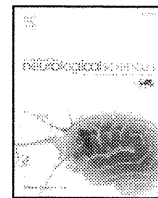
In most cases authors are permitted to post their version of the article (e.g. in Word or Tex form) to their personal website or institutional repository. Authors requiring further information regarding Elsevier's archiving and manuscript policies are encouraged to visit:

<http://www.elsevier.com/copyright>



Contents lists available at ScienceDirect

Journal of the Neurological Sciences

journal homepage: www.elsevier.com/locate/jns

Short communication

Successful treatment with rituximab and thalidomide of POEMS syndrome associated with Waldenstrom macroglobulinemia

Yawara Kawano^{a,1}, Tatsuya Nakama^{b,1}, Hiroyuki Hata^{a,*}, En Kimura^{b,*}, Natsue Maruyoshi^c, Makoto Uchino^b, Hiroaki Mitsuya^a^a Department of Hematology, Kumamoto University Hospital, 1-1-1 Honjo, Kumamoto 860-8556, Japan^b Department of Neurology, Kumamoto University Hospital, 1-1-1 Honjo, Kumamoto 860-8556, Japan^c Department of Neurology, National Hospital Organization Kumamoto South Hospital, 2338 Toyofuku, Matsubase, Uki, Kumamoto, 869-0593, Japan

ARTICLE INFO

Article history:

Received 10 May 2010

Received in revised form 16 June 2010

Accepted 23 June 2010

Available online 31 July 2010

Keywords:

POEMS syndrome

Macroglobulinemia

Rituximab

Thalidomide

IgM- λ type M-proteinemia

ABSTRACT

A POEMS syndrome is a rare disorder characterized by **poly**neuropathy, **organomegaly**, **endocrinopathy**, **monoclonal gammopathy** and **skin abnormalities** including hyperpigmentation and hypertrichosis. Here we report a 55-year-old female case of a POEMS syndrome associated with Waldenstrom macroglobulinemia. The patient had bed-bound polyneuropathy, splenomegaly, IgM- λ type monoclonal (M) protein, elevated λ -type free light chain (FLC), infiltration of CD20-positive lymphoplasmacytic cells in bone marrow, edema and hypertrichosis, and was diagnosed to have an 'atypical' POEMS syndrome associated with macroglobulinemia. Nerve conduction studies and a sural nerve biopsy confirmed a demyelination and axonal degeneration without IgM deposition on myelin sheathes. None of neuron-related auto-antibodies characteristic of IgM paraproteinemic neuropathies was detected in her serum and cerebrospinal fluid. Weekly administration of rituximab (375 mg/m²) combined with thalidomide (50 mg/day) was initiated. By eight weeks of the treatment, the ambulation activity of the patient was restored and her polyneuropathy completely disappeared as determined by clinical symptoms and electrophysiological examinations. This is the first case report presenting a POEMS syndrome associated with WM treated with rituximab and thalidomide. The further examinations of the present case should shed light on the pathogenesis of the 'atypical' POEMS syndrome.

© 2010 Elsevier B.V. All rights reserved.

1. Introduction

A POEMS syndrome is a rare paraneoplastic syndrome characterized by **poly**neuropathy, **organomegaly**, **endocrinopathy**, **monoclonal (M) protein** and **skin abnormalities**. This syndrome is associated with plasma cell dyscrasia, mostly accompanying IgG- λ or IgA- λ paraproteinemia [1]. Reportedly, there have been only a few cases of POEMS syndrome associated with Waldenstrom macroglobulinemia (WM) [2,3].

We report here a rare case presenting symptoms characteristic of POEMS syndrome associated with the infiltration of CD20-positive clonal lymphocytes in bone marrow and hyper-macroglobulinemia, indicating simultaneous occurrence of POEMS syndrome and WM. Improvement of neurological symptoms by the treatment targeting CD20-positive lymphocytes is also described.

2. Case report

A 55-year-old Japanese woman, who had suffered from intense general fatigue, a progressive paresthesia, and peripheral ataxic gait disturbance over the preceding 2 months, was admitted to our hospital. Physical and neurological examination on admission revealed mild conjunctival anemia, cervical lymph nodes swelling (elastic soft, 5 mm each), hepato-splenomegaly, pitting edema of the legs, cutaneous hyper pigmentation and hyper trichosis at her knee joints, hand clumsiness with distal weakness in upper and lower extremities, impaired grip strengths (right 2.5 kg and left 2.0 kg), glove-and-stockings type sensory disturbance, and all her deep tendon reflexes were decreased. She could still stand with someone's help, but disable to walk as of mainly ataxia. Laboratory tests revealed anemia with hemoglobin of 7.5 g/dL. The white blood cell count was 4200/ μ L, consisting 60% of lymphocytes. She had an elevated serum IgM level (4061 mg/dL), while her IgA (4 mg/dL) and IgG (534 mg/dL) levels were markedly low, and also an M-protein was detected by her serum protein electrophoresis. There was no evidence of endocrine abnormality (Table 1). Bone marrow aspiration showed marked infiltration of lymphoplasmacytic cells at a proportion of 60.4% (Fig. 1A). Immunohistochemical staining of her bone marrow showed

* Corresponding authors. Kimura is to be contacted at Tel.: +81 96 373 5893; fax: +81 96 363 5895. Hata, Tel.: +81 96 373 5156; fax: +81 96 363 5265.

E-mail addresses: hata@kumamoto-u.ac.jp (H. Hata), enkimura@kumamoto-u.ac.jp (E. Kimura).

¹ The first 2 authors should be regarded as joint first authors.

Table 1
Laboratory findings and nerve conduction studies during clinical course.

		Before 1st RTM	After 4th RTM	6 mo after 8th RTM	Normal limits
Hb		6.5	12.1	13.5	11.4–15.6 (g/dL)
Plt		1.1	18.2	19.4	13.6–35.2 ($\times 10^4/\mu\text{L}$)
VEGF		265	63	NT	<38.3 (pg/mL)
sIL-2R		3281	557	381	145–519 (U/mL)
IgM		4061	3606	1270	46–260 (mg/dL)
FLC- λ		78.7	53.1	NT	5.7–26.3 (mg/L)
κ/λ		0.08	0.11	NT	0.26–1.65
Ulnar	CMAP	2.5	4.3	7.43	5.0 mV
	MCV	13.1	48.3	64.4	49.9 m/s
	SNAP	NR	0.9	10.60	6.9 μV
	SCV	NR	45.3	55.6	46.8 m/s
Tibial	CMAP	NR	1.3	5.19	4.3 mV
	MCV	NR	29.8	39.4	41.6 m/s

RTM: rituximab, Hb: hemoglobin, Plt: platelet, VEGF: vascular endothelial growth factor, sIL-2R: soluble IL-2 receptor, FLC- λ : serum immunoglobulin free light chain λ , κ/λ : κ and λ ratio, CMAP: compound muscle action potential, MCV: motor conduction velocity, SNAP: sensory neuron action potential, SCV: sensory conduction velocity, NR: not recordable, NT: not tested.

that the lymphoplasmacytic cells were positive for both IgM and λ light chain. Flow cytometry analysis of her bone marrow mononuclear cells revealed the monoclonal proliferation of lymphocytes at a proportion of 44.1%. These monoclonal cells were also positive for CD19, CD20 and Smlg- λ , but negative for CD5 and CD10 (Fig. 1B). There was also an elevation of soluble IL-2 receptor (3281 U/mL), plasma vascular endothelial growth factor (VEGF: 265 pg/mL), and

serum γ immunoglobulin free light chain (FLC, λ chain predominant). None of an anti-myelin-associated glycoprotein (MAG), anti-sulfoluglucuronyl paragloboside (SGPG), or anti-ganglioside IgM/IgG antibodies, characteristic of neural antibodies in IgM paraproteinemic neuropathies [4], was identified. Nerve conduction studies showed low amplitudes of compound muscle action potential (CMAP) and decreases in motor nerve conduction velocity, undetectable sensory

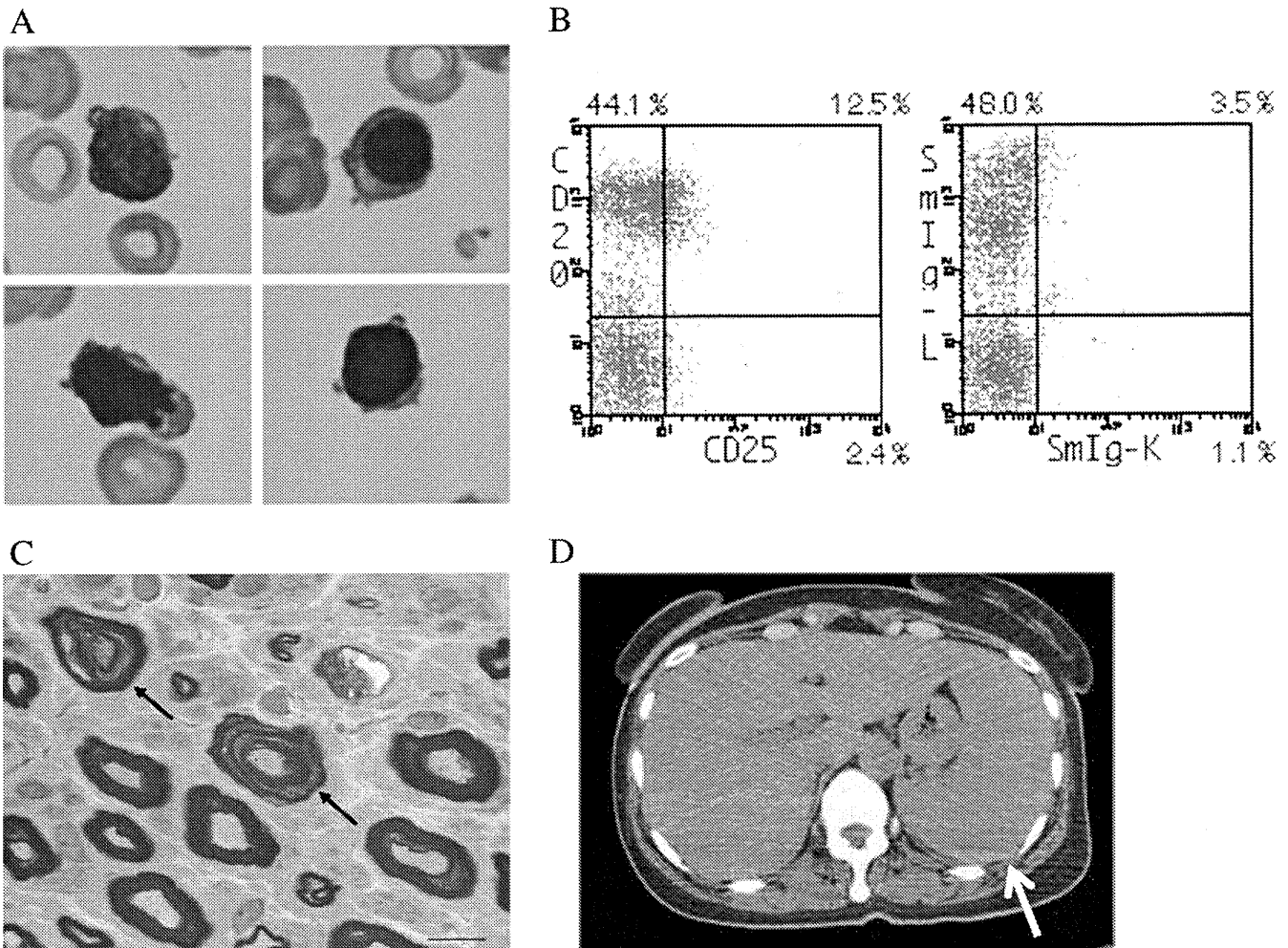


Fig. 1. (A) Morphology of lymphocytes in the bone marrow aspiration sample. Some lymphocytes showed basophilic cytoplasm with slightly eccentric nucleus which indicates a tendency to differentiate into plasma cells. Magnification: 1000 \times , May–Giemsa staining. (B) Flow cytometry analysis of lymphocytes in bone marrow aspiration sample. Clonal proliferation of lymphocytes positive for CD20 and surface Ig- λ was identified. (C) Nerve biopsy showing uncompact myelin lamellae (arrows); toluidine blue staining. (D) Computed tomography scan shows hepatosplenomegaly.